A Thesis

entitled

Fluid Dynamic and Stability Analysis of a Thin Liquid Sheet

by

Matthew S. McMaster

as partial fulfillment of the requirements of

the Master of Science Degree in

Mechanical Engineering

Abdollah A. Afjeh
Advisor

Dean of Graduate School

The University of Toledo

August 1992

THE UNIVERSITY OF TOLEDO

COLLEGE OF ENGINEERING

July 7, 1992

I HEREBY RECOMMEND THAT THE THESIS PREPARED UNDER MY SUPERVISION BY Matthew McMaster

ENTITLED "Fluid Dynamics and Stability of a Thin Liquid Sheet"

BE ACCEPTED IN PARTIAL FULFILLMENT OF THE REQUIREMENTS FOR THE DEGREE OF Master of Science in Mechanical Engineering

Dr. A. Afjeh

Thesis Advisor

Dr. R. K. Irey

Chairman of Discipline

Recommendation concurred in

Committee

on

Final Examination

Acknowledgements

I would like to thank my advisor, Dr. Abdollah A. Afjeh, for his guidance throughout the study. I would also like to thank Dr. Donald L. Chubb for his support and direction throughout the study. Thanks also go out to Larry Cousino, Jose Ayala, and Chris VanCampen for their technical support. I would also like to thank Dr. Masiulaniec and Dr. Ng for serving on my defense committee. And finally, a special thanks to my wife for her assistance and continuous encouragement.

Table of Contents

Notation Table

English Symbols

x, y, z	Orthogonal Cartesian Coordinates
W	Sheet Width
L	Sheet Length
u, v, w	x-, y-, and z- Velocity Components, Respectively
s	Function that Describes the Cross-Sectional Shape of the Edge Cylinder
g	Gravitational Constant
A	Cross-Sectional Area of the Sheet
F	Surface Tension Force
r	Width of the Edge Cylinder
t	Time
Fr	Froude Number
We	Weber Number
P	Pressure
R	Radius of Curvature
U	Dimensionless x-Velocity Component Defined in Equation (2-46)
c	Wave Velocity
k	Axial Wavenumber
X	Dimensionless Sheet Thickness Defined in Equation (3-41)
Y	Dimensionless Frequency Defined in Equation (3-41)

Boldface English Symbols

$\mathbf{v}$	Velocity Vector
$\mathbf{g}$	Gravitational Vector

Greek Symbols

τ	Sheet Thickness
σ	Coefficient of Surface Tension
ρ	Liquid Density
ϕ	Velocity Potential
η	Dimensionless s Defined in Equation (2-46)
ξ	Dimensionless x Defined in Equation (2-46)
ζ	Dimensionless z Defined in Equation (2-46)
α	Proportionality Constant
$\Delta\phi$	Velocity Potential Perturbation
Δs	Shape Function Perturbation
$\hat{\phi}$	Amplitude of the Velocity Potential Perturbation
$\hat{s}$	Amplitude of the Shape Function Perturbation
ω	Frequency
λ	Wavelength
ω'	Frequency Defined in Equation (3-25)
ρ'	Density Defined in Equation (3-26)
ψ	Angle Between the Sheet Edge and Vertical
ψ'	Angle Between Axisymmetric Waves and Vertical
γ	Dimensionless Constant Defined in Equation (3-41)

Boldface Greek Symbols

$\boldsymbol{\tau}$	Stress Tensor

Subscripts

0	At the Top of the Sheet (Chapter 2) or Assumed Solution (Chapter 3)
c	Edge Cylinder
e	Where the Sheet Connects to the Edge Cylinder
s	On the Sheet Surface
x	x-Component or at Constant x
ST	Surface Tension
stag	Stagnation Point
sy	Symmetric
asy	Asymmetric
i	Imaginary
a	Air
CR	Critical

Superscripts

—	Dimensionless

Brackets

$\langle\rangle$	Average

Table of Figures

Chapter 1
Introduction

Thin sheet flows have been a matter of research interest for many years. Sir Geoffrey Taylor has published a series of papers on the dynamics and stability of liquid sheets, [1]. Dombrowski and Fraser have written a paper on the disintegration of expanding cylindrical sheets, such as would be found in a fuel injector, [2]. Related work has been done by Crapper on capillary waves on fluids of infinite depth, [3]. As long ago as 1879, Rayleigh published a paper on the capillary break-up of a cylindrical liquid jet in air, [4]. Interest in thin sheet flows has recently been renewed due to their potential application in space radiators.

1.1 - Historical Perspective

A classic illustration of the methods of hydrodynamic stability is Rayleigh's theory of the break-up of a liquid jet in air, such as the formation of drops by a thin jet of water from a faucet. It had previously been shown that capillarity would lead to instability of a round jet, because an axisymmetric deformation could decrease the surface area of the jet. Rayleigh analyzed in detail the instability of a uniform basic flow of incompressible, inviscid liquid within a cylinder; the liquid having a free surface governed by its surface tension. The jet was found to be stable to all non-axisymmetric modes, but is unstable to axisymmetric modes whose wavelength is greater than the circumference of the jet. Rayleigh's theory agrees well with experiments. Rayleigh also found that there is a

recognized word, varicosity, to describe the axisymmetric instability. This is sometimes called sausage instability now, [4].

In the second paper of Geoffrey Taylor's series he discussed the waves on thin sheets of fluid. He showed that capillary waves are of two kinds, symmetrical waves in which the displacements of opposite sides are in opposite directions, and antisymmetrical waves in which the displacements are in the same direction, as shown by Figure 1-1. Any disturbance can be regarded as composed of these two types of waves. The antisymmetrical waves were shown to be non-dispersive. The antisymmetrical waves in a sheet of uniform thickness caused by a point disturbance were shown to appear as two narrow line-like waves. The symmetrical waves were very different, they were highly dispersive and were propagated much more slowly than the antisymmetrical waves. Experimentally, a point disturbance produces both kinds of waves simultaneously. The

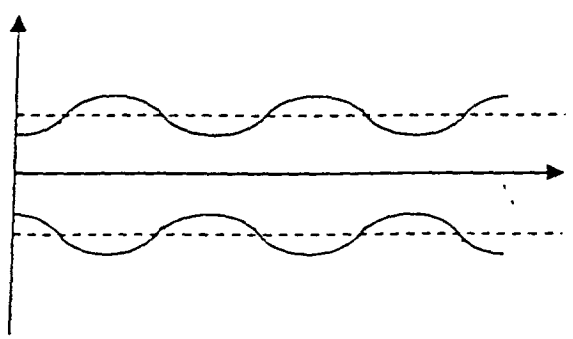

Symmetric Waves

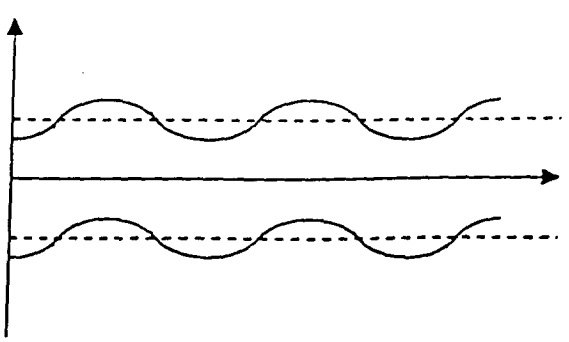

Asymmetric Waves

Figure 1-1 Symmetric and Asymmetric Waves

symmetrical waves in a sheet of uniform thickness caused by a point disturbance were shown to appear as parabolas, [1].

In 1960, D. R. Brown carried out an experimental investigation of thin liquid sheet flow in connection with a method of lacquer application known as curtain coating. In curtain coating, the coating material passes through a thin slit and a liquid sheet is produced. The width of the sheet is maintained by guide wires along the edges of the sheet. The minimum liquid flow rate required to maintain a stable sheet is discussed, and the effects of the impingement of the sheet on a rapidly moving surface are described, [5].

The stability of a viscous liquid curtain falling down steadily under the influence of gravity was investigated by S. P. Lin in 1980. A linear stability analysis was carried out and it was found that only the spatially growing disturbances whose group velocity points toward the upstream direction were unstable. A critical Weber number was found. Any sheet formed with a Weber number less than the critical Weber number was found to be unstable, [6]. This was in good agreement with the experimental results found by Brown.

1.2 - Space Application

One way of significantly reducing the mass of a space radiator is to eliminate the containing walls for the working fluid. Thus the working fluid is exposed to the vacuum condition of space. Such an external flow radiator will have a lower mass than a heat pipe type radiator. Ease of deployment and near immunity to meteoroid damage are two other advantages of external flow radiators.

Currently there are three different designs for external flow radiators. They are the liquid droplet radiator (LDR), the liquid belt radiator (LBR), and the liquid sheet radiator (LSR). The liquid sheet radiator uses a thin liquid sheet as the radiating surface. The sheet may be as thin as 0.0015 in.

The idea behind the design of the liquid sheet radiator is to have the greatest surface area for the least volume or mass. With a very thin liquid sheet the mass is very small, while the surface area, both sides of the sheet, is quite large, allowing for much more specific surface area than the LDR or LBR. Also, being a single sheet, the radiation of heat from one droplet to another droplet is eliminated.

One of the advantages of the LSR is ease of design. The machining required for the fabrication of the narrow slits that are used in producing the sheet does not require as much precision as that for the fabrication of the many small holes for the liquid droplet radiator. Also, the pump power will be less since the viscous losses for a single slit are less than that for many small holes. Collection of the liquid is also greatly simplified since the sheet coalesces to a single point, as will be shown later. The simpler design for the sheet generator and collector should result in a lower mass for these components, [7].

Due to its many advantages the LSR has been the subject of great interest in recent years. This has resulted in the need to fully understand the fluid dynamics and stability of a thin liquid sheet.

1.3 - Introduction to Liquid Sheet Flow

A liquid sheet is formed by forcing the working fluid through a very thin slit. Since the sheet is so thin, the surface tension has a very pronounced effect. The sheet edges are pulled towards the center of the sheet, (see Figure 1-2). This causes the sheet to take on a triangular form. Due to conservation of mass the fluid must collect in the so-called edge cylinders that border the sides of the sheet.

In order to more fully understand the fluid dynamics of liquid sheet flow, a number of analytical and experimental studies were carried out. The first analytical study, Chapter 2 Section 1, was to determine an analytical prediction for the sheet length over slit width ratio for the liquid sheet. The second, Chapter 2 Section 2, was to determine the theoretical

Figure 1-2 Photograph of a Thin Liquid Sheet

cross-sectional shape of the edge cylinders.

In addition to the fluid dynamics of liquid sheet flow it is also of vital importance to understand the stability of the flow. This is the focus of Chapter 3. In Chapter 3, a linear stability analysis is presented on a non-planer liquid jet. This analysis shows the possible instability of the edge cylinders.

Chapter 4 has two main parts. In the first part, the experimental apparatus is described. In the second part, the formation of holes in the sheet is discussed and the method of eliminating those holes is presented.

Chapters 5 and 6 present the experimental procedures and the experimental results, respectively. Experiments were carried out to measure the length over width ratios for the liquid sheet and comparisons were made to the theoretical predictions presented in Chapter 2. An elaborate photographic technique was employed in order to determine the cross-sectional shape of the edge cylinders. This experiment revealed a very interesting phenomenon, the edge cylinder cross-sectional shape oscillates between an elliptical and a peanut-like shape, and the theoretical predictions are only valid in the limiting case. A third experimental study was performed on the effects of air drag on a liquid sheet.

1.4 - Introduction to Linear Stability Analysis

The essential problems of hydrodynamic stability were recognized and formulated in the nineteenth century, notably by Helmholtz, Kelvin, Rayleigh and Reynolds. The method of normal modes for studying the oscillations and instability of a dynamic system of particles and rigid bodies was already highly developed. A known solution of Newton's or Lagrange's equation of motion for the system was perturbed. The equations were linearized by neglecting products of the perturbations. It was further assumed that the perturbation of each quantity could be resolved into independent components or modes varying with time t, like e^{st} for some constant s, which is in general complex. The values of s for the modes were calculated from the linearized equations. If the real part of s was found to be positive for any mode, the system was deemed unstable because a general initial small perturbation of the system would grow exponentially in time.

Stokes, Kelvin, and Rayleigh adapted this method of normal modes to fluid dynamics. The essential mathematical difference between fluid and particle dynamics is

that the equations of motion are partial rather than ordinary differential equations. This difference leads to many mathematical difficulties in hydrodynamic stability, which have been overcome for only a few classes of flow with very simple configurations.

Chapter 2
Theoretical Formulation

The focus of this chapter is to analytically determine the sheet length over slit width ratio and the cross-sectional shape of the edge cylinders. A better understanding of the problem at hand can be realized by referring to Figure 2-1, where the front and cross-sectional views of the liquid sheet are shown schematically. The sheet is formed by forcing the working fluid through a very thin slit, of length W_0 and thickness τ_0. The sheet is then pulled together by surface tension until the sheet coalesces at a length L. An orthogonal-cartesian coordinate system centered at the top of the sheet in the middle of the slit is adopted. The z-axis points in the vertical down direction, the x-axis points to the right along the slit, and the y-axis goes in the direction of the thickness of the sheet. The velocity convention that u, v, and w denote the x, y, and z components of velocity, respectively, will be used throughout the chapter. Moreover, s(x,z) represents the function that will describe the cross-sectional shape of the edge cylinders. Using the above mentioned notation, the two objectives of this chapter are to determine L/W_0 and s(x,z).

In the following section the effects of gravity and surface tension on the sheet will be considered. First, the forces acting on the edge cylinder will be considered, resulting in an expression for the velocity of the edge in the x-direction. Second, a macroscopic mass balance on the entire sheet will be undertaken to determine the sheet length over slit width ratio. Third, the sheet length over slit width ratio will be found by neglecting gravity and compared to the ratio that included the effects of gravity. This analysis will result in showing that the surface tension is the dominating force in the sheet and that the gravitational force may be neglected.

In the second section the only force acting on the sheet will be the surface tension force. Here, the equations of continuity and motion will be solved to obtain the cross-sectional shape of the edge cylinders. A number of assumptions will be made resulting in the motion equation just being a balance of inertial forces and surface tension forces. The objective is to develop a method for predicting the shape of the edge cylinder from knowing the area of the edge cylinder. This area, in turn, can be found from the results of the first section.

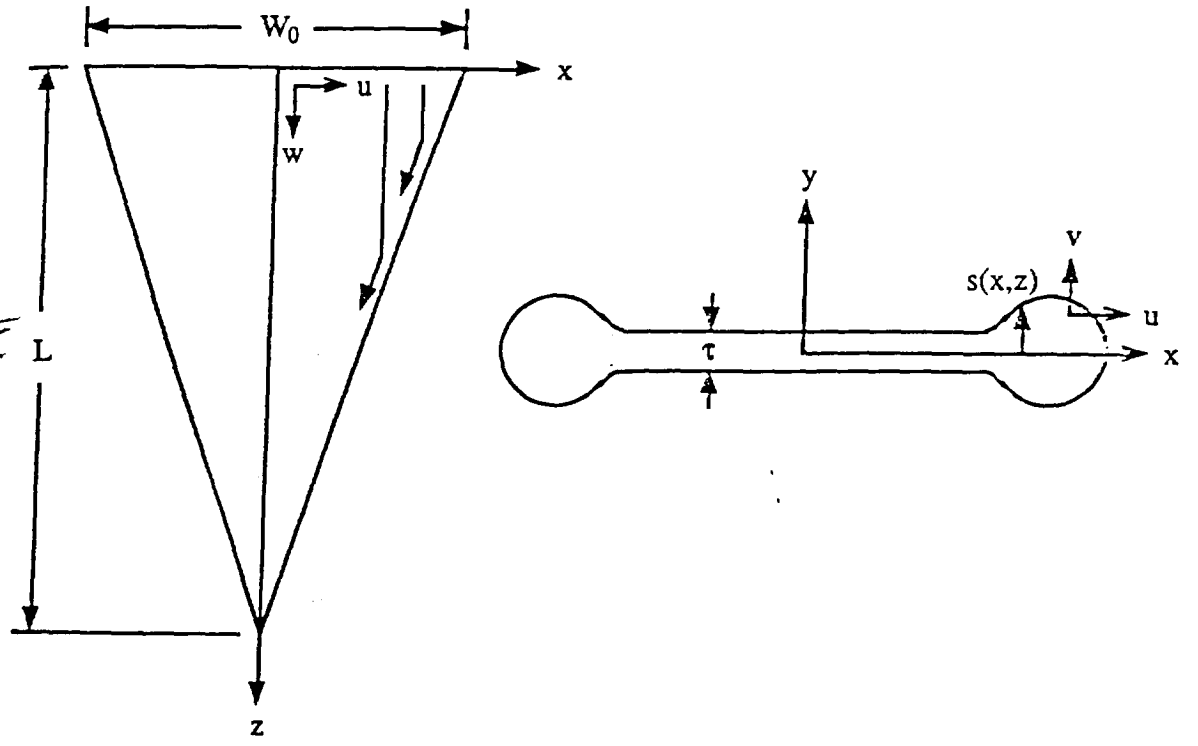

Front View Cross-Sectional View

Figure 2-1 Schematic of Thin Sheet Flow

2.1 - Derivation of the Sheet Length over Slit Width Ratio

2.1.1 - Development of the Governing Equations

Consider an arbitrary element of the edge cylinder with a thickness of dz, as shown in Figure 2-2. Let this element be considered a control volume. Assume it to be at pseudo-steady state, that is, it will be considered steady when conservation of momentum is applied and unsteady when conservation of mass is applied. Furthermore assume it to be unaffected by gravity. Assuming a zero slope at the point where the cylinder connects to the sheet, the surface tension force between the cylinder and the sheet is σdz for both the front and the back of the sheet, therefore:

$$dF_x = 2\sigma dz$$

or

$$\frac{dF_x}{dz} = 2\sigma$$

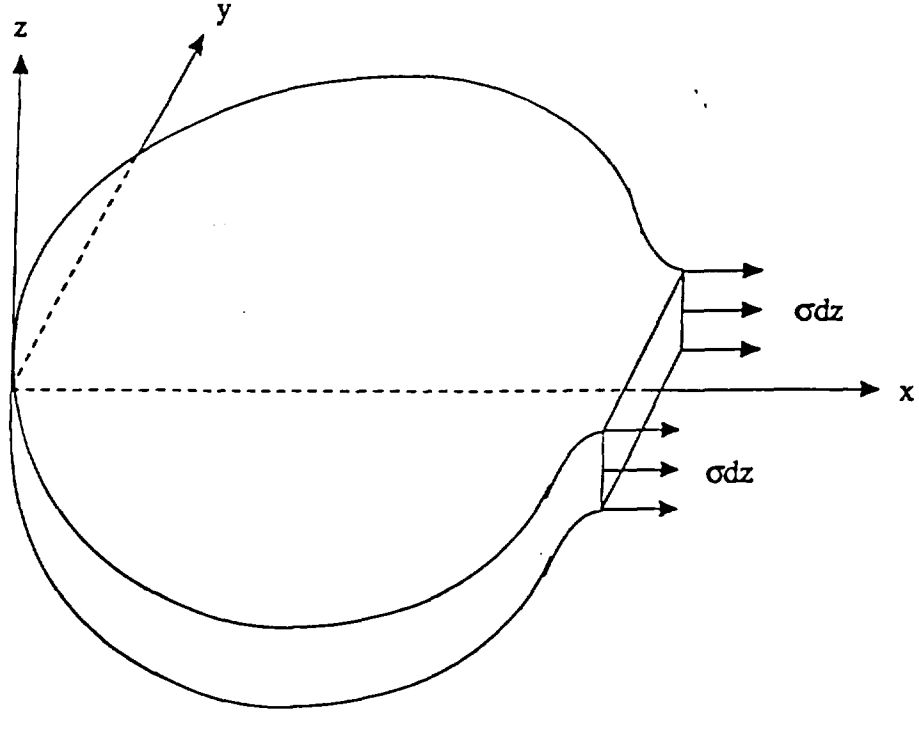

Figure 2-2 Differential Element of the Edge Cylinder

Let u_e be equal to the velocity at which fluid enters the control volume at the right edge. Applying a macroscopic momentum balance on this control volume yields:

$$dF_x = \rho u_e^2 \tau dz$$

or:

$$\rho u_e^2 \tau = \frac{dF_x}{dz} = 2\sigma$$

Therefore:

$$u_e = \sqrt{\frac{2\sigma}{\rho\tau}} \tag{2-1}$$

If A_c is defined as the area in the xy plane of the control volume, then applying a macroscopic mass balance on the control volume yields:

$$\frac{d}{dt}(\rho A_c dz) = \rho u_e \tau dz$$

Therefore:

$$\frac{dA_c}{dt} = \tau u_e = \sqrt{\frac{2\sigma\tau}{\rho}} \tag{2-2}$$

If the principle of conservation of mass is applied to the entire sheet (see Figure 2-1) then it can be shown that:

$$\rho w_0 W_0 \tau_0 = \rho w(2A_c + W\tau)$$

Since the fluid is incompressible and assuming $\tau w = \tau_0 w_0$, the above equation can be written as:

$$w_0 W_0 \tau_0 = 2wA_c + w_0 \tau_0 W \tag{2-3}$$

Since the change with time of the sheet width is twice the edge velocity it may be written that:

$$\frac{dW}{dt} = -2u_e = -\sqrt{\frac{8\sigma}{\rho\tau}} \tag{2-4}$$

It is known that the acceleration in the z-direction is due to gravity or:

$$\frac{d^2z}{dt^2} = \frac{dw}{dt} = g \tag{2-5}$$

Integrating, knowing that at t = 0; dz/dt = w_0, gives:

$$\frac{dz}{dt} = w = gt + w_0 \tag{2-6}$$

Taking equation (2-3) and differentiating with respect to time yields:

$$0 = 2\frac{dA_c}{dt}w + 2A_c\frac{dw}{dt} + \tau_0 w_0\frac{dW}{dt}$$

Differentiating again yields:

$$0 = 2\frac{d^2A_c}{dt^2}w + 4\frac{dA_c}{dt}\frac{dw}{dt} + 2A_c\frac{d^2w}{dt^2} + \tau_0 w_0\frac{d^2W}{dt^2}$$

But,

$$\frac{d^2w}{dt^2} = \frac{dg}{dt} = 0$$

Resulting in:

$$0 = 2\frac{d^2A_c}{dt^2}w + 4\frac{dA_c}{dt}\frac{dw}{dt} + \tau_0 w_0\frac{d^2W}{dt^2} \tag{2-7}$$

Differentiating equations (2-2) and (2-4) with respect to time gives:

$$\frac{d^2A_c}{dt^2} = \sqrt{\frac{\sigma}{2\rho\tau}}\frac{d\tau}{dt} \tag{2-8}$$

$$\frac{d^2W}{dt^2} = \sqrt{\frac{2\sigma}{\rho\tau^3}}\frac{d\tau}{dt} \tag{2-9}$$

Substituting equations (2-2), (2-5), (2-6), (2-8), and (2-9) into equation (2-7) yields:

$$0 = 2\sqrt{\frac{\sigma}{2\rho\tau}}\frac{d\tau}{dt}(gt + w_0) + 4\sqrt{\frac{2\sigma\tau}{\rho}}g + \tau_0 w_0\sqrt{\frac{2\sigma}{\rho\tau^3}}\frac{d\tau}{dt}$$

Solving this for dτ/dt gives:

$$\frac{d\tau}{dt} = \frac{-4\tau^2 g}{\tau(gt + w_0) + \tau_0 w_0} \tag{2-10}$$

From this expression it is apparent that if g = 0 the thickness is constant, as would be the case in space application. But, since g is greater than 0, dτ/dt is less than 0 and the sheet becomes thinner.

Introduce the following dimensionless variables:

$$\overline{W} = \frac{W}{W_0}; \bar{z} = \frac{z}{W_0}; \bar{\tau} = \frac{\tau}{\tau_\theta}; \bar{t} = \frac{tw_0}{W_0}; \overline{w} = \frac{w}{w_0} \tag{2-11}$$

Rewriting equation (2-10) in terms of the new dimensionless variables yields:

$$\frac{d\bar{\tau}}{d\bar{t}} = -\frac{4\bar{\tau}^2}{\frac{w_0^2}{W_0 g} + \frac{w_0^2}{W_0 g}\left(\frac{\bar{\tau} g W_0 \bar{t}}{w_0^2} + \bar{\tau}\right)}$$

Or, in terms of the Froude number, defined as the ratio of inertial forces to gravitational forces:

$$Fr = \frac{w_0^2}{gW_0} \tag{2-12}$$

One obtains:

$$\frac{d\bar{\tau}}{d\bar{t}} = -\frac{4\bar{\tau}^2}{Fr\left(1 + \bar{\tau}\left(\frac{\bar{t}}{Fr} + 1\right)\right)}$$

For the special case of small $\bar{t}$/Fr it is permissible to neglect it, giving:

$$\frac{d\bar{\tau}}{d\bar{t}} = -\frac{4\bar{\tau}^2}{Fr\left(1 + \bar{\tau}\right)} \tag{2-13}$$

Rearranging and integrating results in an equation for $\bar{\tau}$ as a function of $\bar{t}$.

$$\int \frac{(\bar{\tau} + 1)d\bar{\tau}}{\bar{\tau}^2} = -\frac{4}{Fr}\int d\bar{t}$$

$$\ln\bar{\tau} - \frac{1}{\bar{\tau}} = -\frac{4}{Fr}\bar{t} + c$$

Using the boundary condition that at $\bar{t} = 0$; $\bar{\tau} = 1$ it can be seen that c = -1 and:

$$\bar{t} = \frac{Er}{4}\left(\frac{1}{\bar{\tau}} - \ln\bar{\tau} - 1\right) \tag{2-14}$$

Writing equation (2-4) in terms of the previous dimensionless variables results in:

$$\frac{d\overline{W}}{d\bar{t}} = -\sqrt{\frac{8\sigma}{w_0^2\rho\tau_0\bar{\tau}}}$$

Incorporating the Weber number, defined as the ratio of inertial forces to surface tension forces,

$$We = \frac{\rho w_0^2 \tau_0}{\sigma} \tag{2-15}$$

one obtains.

$$\frac{d\overline{W}}{d\bar{t}} = -\sqrt{\frac{8}{We\bar{\tau}}} \tag{2-16}$$

If equation (2-13) is divided by equation (2-16) an expression for $d\bar{\tau}/d\overline{W}$ can be obtained.

$$\frac{d\bar{\tau}}{d\bar{t}}\frac{d\bar{t}}{d\overline{W}} = \frac{-4\bar{\tau}^2}{-\sqrt{\frac{8}{We\bar{\tau}}}\,Fr\left(1+\bar{\tau}\right)}$$

$$\frac{d\bar{\tau}}{d\overline{W}} = \frac{\sqrt{2We}\,\bar{\tau}^{5/2}}{Fr\left(1+\bar{\tau}\right)}$$

This can be integrated to find $\overline{W}(\bar{\tau})$

$$\int \frac{\left(1+\bar{\tau}\right)d\bar{\tau}}{\bar{\tau}^{5/2}} = \frac{\sqrt{2We}}{Fr}\int d\overline{W}$$

$$-\frac{2}{3}\bar{\tau}^{-3/2} - 2\bar{\tau}^{-1/2} = \frac{\sqrt{2We}}{Fr}\overline{W} + c$$

$$\overline{W} = \frac{Fr}{\sqrt{2We}}\left(c - \frac{2}{3}\bar{\tau}^{-3/2} - 2\bar{\tau}^{-1/2}\right)$$

Using the boundary condition that at $\overline{W} = 1$; $\bar{\tau} = 1$, it is found that:

$$c = \frac{\sqrt{2We}}{Fr} + \frac{8}{3}$$

Therefore:

$$\overline{W} = \frac{Fr}{\sqrt{2We}}\left(\frac{\sqrt{2We}}{Fr} + \frac{8}{3} - \frac{2}{3}\bar{\tau}^{-3/2} - 2\bar{\tau}^{-1/2}\right)$$

or

$$\overline{W} = 1 - \frac{Fr}{3}\sqrt{\frac{2}{We}}\left(\bar{\tau}^{-3/2} + 3\bar{\tau}^{-1/2} - 4\right) \qquad (2\text{-}17)$$

Writing equation (2-6) in terms of the dimensionless variables introduced earlier, yields:

$$\frac{d\bar{z}}{d\bar{t}} = \frac{gW_0}{w_0^2}\bar{t} + 1$$

or

$$\frac{d\bar{z}}{d\bar{t}} = \frac{\bar{t}}{Fr} + 1$$

Integration yields $\bar{z}(\bar{t})$:

$$\int d\bar{z} = \int \left(\frac{\bar{t}}{Fr} + 1\right) d\bar{t}$$

$$\bar{z} = \frac{1}{2Fr}\bar{t}^2 + \bar{t} + c$$

Applying the boundary condition, at $\bar{t} = 0$; $\bar{z} = 0$, results in $c = 0$, therefore:

$$\bar{z} = \frac{1}{2Fr}\bar{t}^2 + \bar{t} \qquad (2\text{-}18)$$

In order to find the sheet length over slit width ratio, L/W_0, equation (2-17) should be solved for $\bar{\tau}$ numerically when $\overline{W} = 0$. This value for $\bar{\tau}$ can then be plugged into equation (2-14) to find $\bar{t}$. Finally, the value for $\bar{t}$ can be plugged into equation (2-18) to find $\bar{z}$. The resulting value for $\bar{z}$ is the sheet length over slit width ratio for the given flow parameters.

The value for L/W_0 can be determined much more easily and without the aid of the computer if gravity is neglected, as is the case in space application. As was shown before,

if $g = 0$ then $d\bar{\tau}/d\bar{t} = 0$, and consequently $\bar{\tau} = 1$ throughout the sheet. Thereby equation (2-16) can be written as:

$$\frac{d\overline{W}}{d\bar{t}} = -\sqrt{\frac{8}{We}}$$

This can be integrated to find $\overline{W}$ as a function of $\bar{t}$:

$$\int d\overline{W} = -\sqrt{\frac{8}{We}} \int d\bar{t}$$

$$\overline{W} = -\sqrt{\frac{8}{We}}\,\bar{t} + c$$

From the boundary condition, $\bar{t} = 0$; $\overline{W} = 1$, it can be seen that $c = 1$ and:

$$\overline{W} = -\sqrt{\frac{8}{We}}\,\bar{t} + 1$$

Now, $\overline{W}$ can be set equal to zero to solve for $\bar{t}$, giving:

$$\bar{t} = \sqrt{\frac{We}{8}}$$

Since, when $g = 0$ the Froude number is equal to infinity, equation (2-18) may be rewritten as:

$$\bar{z} = \bar{t}$$

Therefore:

$$\bar{z} = \sqrt{\frac{We}{8}} \qquad (2\text{-}19)$$

Therefore, the L/W_0 ratio in zero gravity, is simply equal to $\sqrt{\frac{We}{8}}$.

2.1.2 - Computer Solution

The Fortran program FLUDYN has been written to compute the L/W_0 ratios for a typical range of Froude and Weber numbers. This program computes the L/W_0 ratios both including the effect of gravity and neglecting it. The results of this program have shown a

negligible difference (<0.1%) in the calculated L/W_0 ratios if gravity effects are considered. For this reason, the rest of the calculation for the cylinder cross-sectional shape shall be done by neglecting the force of gravity.

The text of FLUDYN can be found in Appendix B. Figure 2-3 shows how $\overline{W}$ and $\bar{\tau}$ vary with $\bar{z}$ for a Weber number of 20. This shows how the sheet becomes thinner on the way down and how it keeps a basically triangular shape under the influence of gravity. The choice of Weber number equal to 20 was to show the sheet thinning, as the Weber number gets higher this effect becomes less and less. Figure 2-4 shows the sheet length over slit width ratios versus the Weber number. These were calculated without the effect of gravity. Those values that were calculated with the effect of gravity could have been plotted but the difference would not have been noticeable.

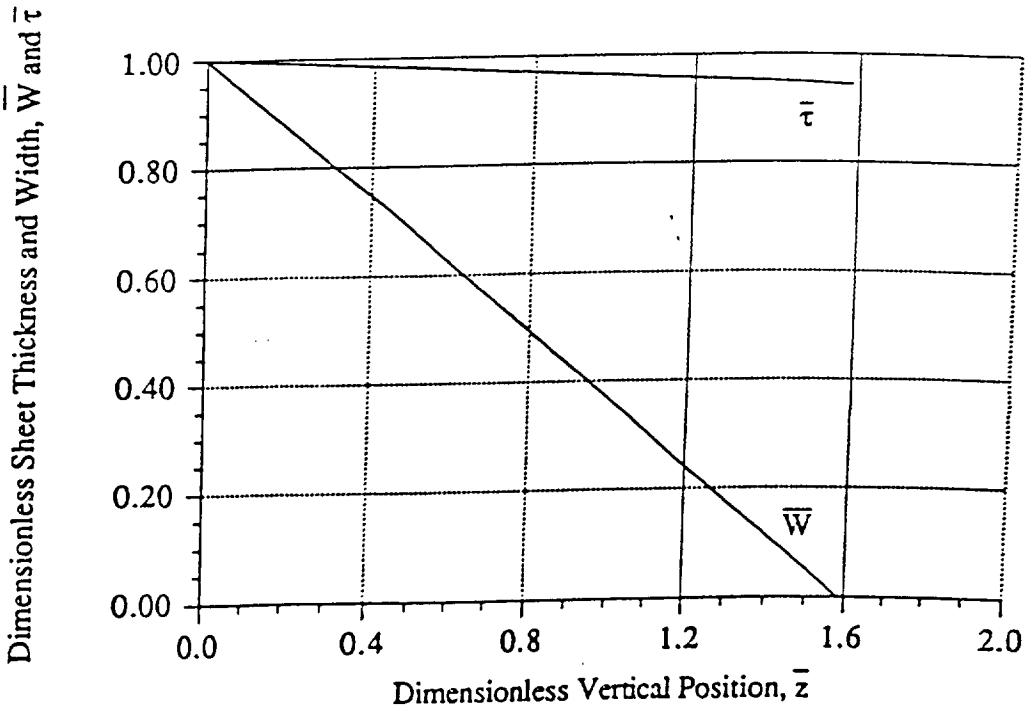

Figure 2-3 Sheet Width and Thickness vs. Vertical Position for We = 20.0

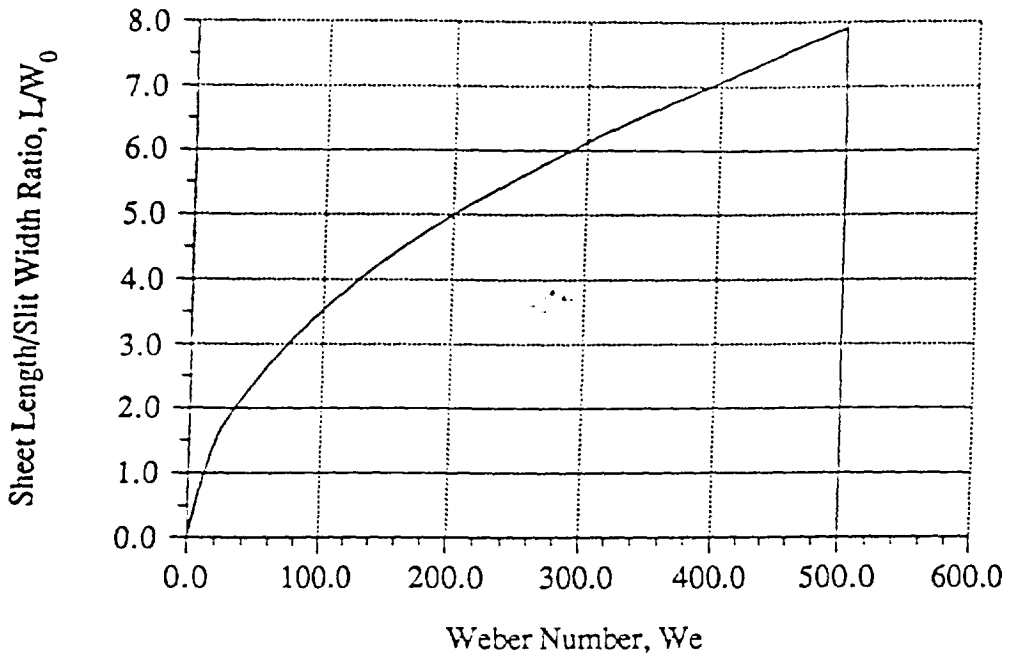

Figure 2-4 Sheet Length/Sheet Width Ratio vs. Weber Number

2.2 - Derivation of the Edge Cylinder Cross-Sectional Shape

The full equations of continuity and motion, including the surface tension pressure, are as follows (see Appendix A):

Continuity:

$$\frac{\partial \rho}{\partial t} = -\left(\nabla \cdot \rho \mathbf{v}\right) \tag{2-20}$$

Motion:

$$\frac{\partial}{\partial t}\rho \mathbf{v} = -\nabla \cdot \rho \mathbf{v}\mathbf{v} - \nabla(P_a + P_{ST}) - \nabla \cdot \tau + \rho g \tag{2-21}$$

Several assumptions need to be made to simplify these equations.

1) The flow is steady state;

2) The fluid is incompressible;

3) Gravity is neglected;

4) The fluid is inviscid;

5) Air pressure gradient is neglected;

6) The flow is irrotational;

As a consequence of these assumptions,

$$\frac{\partial \rho}{\partial t} = \frac{\partial}{\partial t}\rho \mathbf{v} = 0$$

$$\rho = \text{constant}$$

$$\mathbf{g} = \tau = 0$$

$$\nabla P_a = 0$$

$$\nabla \times \mathbf{v} = 0$$

and the governing equations reduce to,

Continuity:

$$\nabla \cdot \mathbf{v} = 0$$

Motion:

$$\nabla \cdot \mathbf{v}\mathbf{v} + \frac{\nabla P_{ST}}{\rho} = 0$$

Through the use of vector identities, the equation of continuity, and the irrotationality assumption, the first term in the equation of motion can be simplified.

$$\nabla \cdot \mathbf{v}\mathbf{v} = \mathbf{v} \cdot \nabla \mathbf{v} + \mathbf{v}(\nabla \cdot \mathbf{v}) = \mathbf{v} \cdot \nabla \mathbf{v} = \frac{1}{2}\nabla(\mathbf{v} \cdot \mathbf{v}) - \mathbf{v} \times (\nabla \times \mathbf{v}) = \frac{1}{2}\nabla(\mathbf{v} \cdot \mathbf{v}) = \frac{1}{2}\nabla v^2$$

Therefore,

Continuity:

$$\nabla \cdot \mathbf{v} = 0 \qquad (2\text{-}22)$$

Motion:

$$\frac{1}{2}\nabla v^2 + \frac{\nabla P_{ST}}{\rho} = 0 \qquad (2\text{-}23)$$

2.2.1 - Integral Formulation of the Continuity Equation

Consider Figure 2-5 showing a typical cross-sectional shape and the coordinate system to be used. The function s(x,z) describes the cross-sectional shape. The function r(z) is essentially the width of the edge shape, and is defined as the point where $s = \tau_0/2$ and $u = -u_e$.

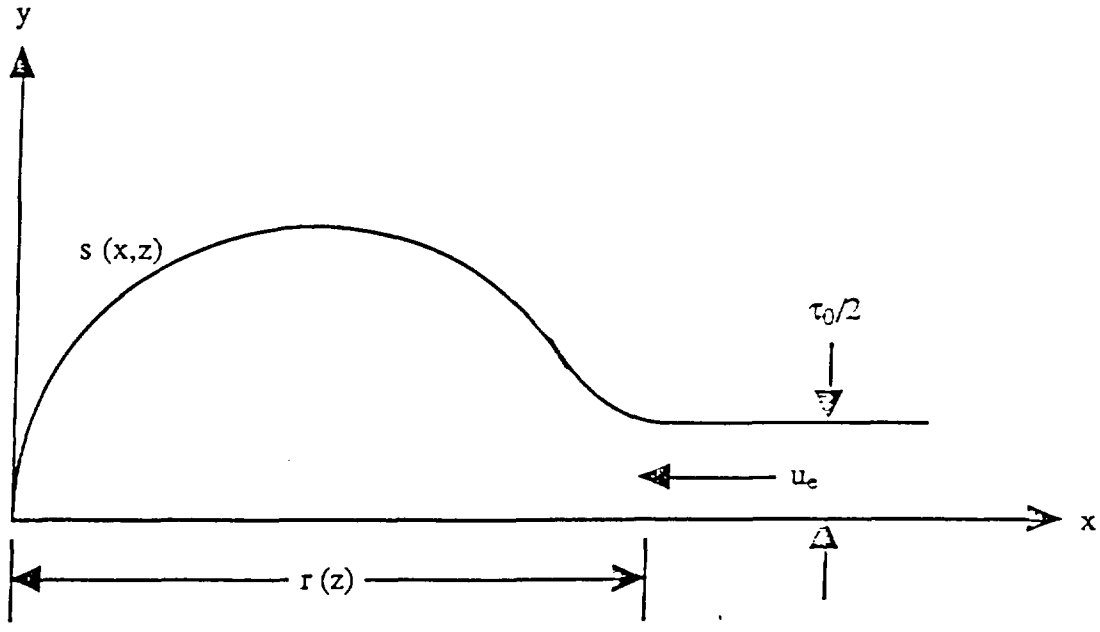

Figure 2-5 Typical Edge Cylinder Cross-Sectional Shape

Expanding the continuity equation for this control volume yields:

$$\frac{\partial u}{\partial x} + \frac{\partial v}{\partial y} = 0 \qquad (2\text{-}24)$$

Integrating equation (2-24) from 0 to s over y gives:

$$\int_0^s \left(\frac{\partial u}{\partial x} + \frac{\partial v}{\partial y}\right) dy = 0$$

or:

$$\int_0^s \frac{\partial}{\partial x}(udy) + \int_0^s \frac{\partial}{\partial y}(vdy) = 0 \tag{2-25}$$

The second integral in equation (2-25) may be directly integrated. Knowing that v at y = 0 is equal to 0 due to the symmetry of the sheet,

$$\int_0^s \frac{\partial}{\partial y}(vdy) = v_{s,} - v_{y=0} = v_s \tag{2-26}$$

The first integral in equation (2-25) may be evaluated through the use of Leibnitz's rule.

$$\int_0^s \frac{\partial}{\partial x}(udy) = \frac{\partial}{\partial x}\int_0^s udy - \left(u_s \frac{\partial s}{\partial x} - u_{y=0}\frac{\partial}{\partial x}(0)\right) = \frac{\partial}{\partial x} s\left(\frac{1}{s}\int_0^s udy\right) - u_s \frac{\partial s}{\partial x}$$

If $\langle u \rangle$ is defined as the average x-component of velocity over y, then:

$$\langle u \rangle = \frac{1}{s}\int_0^s udy \tag{2-27}$$

and,

$$\int_0^s \frac{\partial}{\partial x}(udy) = \frac{\partial}{\partial x} s\langle u \rangle - u_s \frac{\partial s}{\partial x} \tag{2-28}$$

Substituting the integrals in equations (2-26) and (2-28) into the integrated continuity equation, equation (2-25), gives:

$$\frac{\partial}{\partial x} s\langle u \rangle - u_s \frac{\partial s}{\partial x} + v_s = 0 \tag{2-29}$$

Since s = s(x,z) it may be written that:

$$\frac{ds}{dt} = \frac{\partial s}{\partial x}\left(\frac{dx}{dt}\right) + \frac{\partial s}{\partial z}\left(\frac{dz}{dt}\right)$$

It can be seen that for this case:

$$\frac{dx}{dt} = u_s$$

$$\frac{dz}{dt} = w_s = w_0$$

$$\frac{ds}{dt} = \frac{dy}{dt} =$$

Therefore:

$$v_s = u_s \frac{\partial s}{\partial x} -$$ (2-30)

Substituting this relation for v_s into equation gives:

$$\frac{\partial}{\partial x} s\langle u\rangle - u_s \frac{\partial s}{\partial x} + u_s$$ $$= 0$$

or:

$$\frac{\partial}{\partial x} s\langle u\rangle =$$ (2-31)

If equation (2-31) is integrated from 0 to x it is

$$\int_0^x \frac{\partial}{\partial x} s\langle u\rangle dx =$$ (2-32)

The first integral in equation (2-32) may be determined, knowing that at x = 0;

$\langle u\rangle = s = 0$. Therefore:

$$\int_0^x \frac{\partial}{\partial x} s\langle u\rangle dx = (s\langle u\rangle)_x -$$ $$(s\langle u\rangle)_x$$ (2-33)

The second integral in equation (2-32) may be evaluated through the use of Liebnitz's rule.

$$\int_0^x \frac{\partial s}{\partial z} dx = \frac{d}{dz}\int_0^x s dx - \left(s_x \frac{dx}{dz} -$$ $$0\right) = \frac{d}{dz}\int_0^x s dx$$ (2-34)

If equations (2-33) and (2-34) are substituted back into equation (2-32) it yields:

$$(s\langle u\rangle)_x = -w_0 \frac{d}{dz}\int_0^x$$ (2-35)

If A is defined as the cross-sectional area of the sheet from x = 0 to x = x for any z then:

$$A = 2\int_0^x s\,dx \tag{2-36}$$

and

$$(s\langle u\rangle)_x = -\frac{w_0}{2}\left(\frac{dA}{dz}\right)_x \tag{2-37}$$

If A_c is equal to the cross-sectional area of the edge cylinder then:

$$A_c = 2\int_0^r s\,dx \tag{2-38}$$

If the equation (2-37) is applied with x = r, refer to Figure 2-5, then:

$$s = \frac{\tau_0}{2}$$

$$\langle u\rangle = -u_e = -\sqrt{\frac{2\sigma}{\rho\tau_0}}$$

$$A = A_c$$

Therefore:

$$-\frac{\tau_0}{2}\sqrt{\frac{2\sigma}{\rho\tau_0}} = -\frac{w_0}{2}\frac{dA_c}{dz}$$

$$\tau_0\sqrt{\frac{2\sigma}{\rho w_0^2\tau_0}}\,dz = dA_c$$

$$\tau_0\sqrt{\frac{2}{We}}\,dz = dA_c \tag{2-39}$$

Equation (2-39) can be integrated giving:

$$\tau_0\sqrt{\frac{2}{We}}\int dz = \int dA_c$$

$$A_c = \tau_0\sqrt{\frac{2}{We}}\,z + c$$

Knowing that when $z = 0$; $A_c = 0$ it can be seen that $c = 0$ and:

$$A_c = \tau_0 z \sqrt{\frac{2}{We}} \tag{2-40}$$

2.2.2 - Formulation of the Motion Equation

The motion equation can be written for any two points on the surface of the sheet. Let the first point be any arbitrary point, s, on the surface. Let the second point be the stagnation point in the center of the sheet on the surface, where $u = v = 0$. Writing equation (2-23) for these two points yields, (see Appendix A):

$$\frac{1}{2}\rho\left[u_s^2 + v_s^2 + w_0^2\right] - \sigma\left[\frac{\frac{\partial^2 s}{\partial x^2} + \frac{\partial^2 s}{\partial z^2}}{\left[1 + \left(\frac{\partial s}{\partial x}\right)^2 + \left(\frac{\partial s}{\partial z}\right)^2\right]^{\frac{3}{2}}}\right]_s =$$

$$\frac{1}{2}\rho\left[u_{stag}^2 + v_{stag}^2 + w_0^2\right] - \sigma\left[\frac{\frac{\partial^2 s}{\partial x^2} + \frac{\partial^2 s}{\partial z^2}}{\left[1 + \left(\frac{\partial s}{\partial x}\right)^2 + \left(\frac{\partial s}{\partial z}\right)^2\right]^{\frac{3}{2}}}\right]_{stag}$$

or:

$$\frac{1}{2}\rho\left[u_s^2 + v_s^2\right] - \sigma\left[\frac{\frac{\partial^2 s}{\partial x^2} + \frac{\partial^2 s}{\partial z^2}}{\left[1 + \left(\frac{\partial s}{\partial x}\right)^2 + \left(\frac{\partial s}{\partial z}\right)^2\right]^{\frac{3}{2}}}\right]_s = -\sigma\left[\frac{\frac{\partial^2 s}{\partial x^2} + \frac{\partial^2 s}{\partial z^2}}{\left[1 + \left(\frac{\partial s}{\partial x}\right)^2 + \left(\frac{\partial s}{\partial z}\right)^2\right]^{\frac{3}{2}}}\right]_{stag} \tag{2-41}$$

Since all of the partial derivatives on the right hand side of equation (2-41) are taken at the stagnation point, all of them are constant. Therefore the right hand side is equal to a constant, or:

$$\frac{1}{2}\rho\left[u_s^2 + v_s^2\right] - \sigma\left[\frac{\frac{\partial^2 s}{\partial x^2} + \frac{\partial^2 s}{\partial z^2}}{\left[1 + \left(\frac{\partial s}{\partial x}\right)^2 + \left(\frac{\partial s}{\partial z}\right)^2\right]^{\frac{3}{2}}}\right]_s = \frac{\sigma}{R_{stag}} \tag{2-42}$$

From the integral continuity section it was shown that on the surface:

$$v_s = u_s \frac{\partial s}{\partial x} + w_0 \frac{\partial s}{\partial z} \tag{2-30}$$

Since $\partial s/\partial z$ is expected to be small it may be neglected from equations (2-42) and (2-30). Giving:

$$\frac{1}{2}\rho\left[u_s^2 + v_s^2\right] - \sigma\left[\frac{\frac{\partial^2 s}{\partial x^2} + \frac{\partial^2 s}{\partial z^2}}{\left[1 + \left(\frac{\partial s}{\partial x}\right)^2\right]^{\frac{3}{2}}}\right]_s = \frac{\sigma}{R_{stag}} \tag{2-43}$$

and:

$$v_s = u_s \frac{\partial s}{\partial x} \tag{2-44}$$

Substituting equation (2-44) into equation (2-43) and dropping the redundant s subscript gives:

$$\frac{1}{2}\rho\left[u_s^2 + u_s^2\left(\frac{\partial s}{\partial x}\right)^2\right] - \sigma\left[\frac{\frac{\partial^2 s}{\partial x^2} + \frac{\partial^2 s}{\partial z^2}}{\left[1 + \left(\frac{\partial s}{\partial x}\right)^2\right]^{\frac{3}{2}}}\right] = \frac{\sigma}{R_{stag}} \tag{2-45}$$

Define the following dimensionless variables:

$$\eta = \frac{2s}{\tau_0};\ \xi = \frac{2x}{\tau_0};\ \zeta = \frac{2z}{\tau_0};\ \bar{r} = \frac{2r}{\tau_0};\ U_s = \frac{u_s}{u_e} \tag{2-46}$$

Rewriting equation (2-45) in terms of these dimensionless variables gives:

$$\frac{1}{2}\rho\left[U_s^2\left(\frac{2\sigma}{\rho\tau_0}\right) + U_s^2\left(\frac{2\sigma}{\rho\tau_0}\right)\left(\frac{\partial\eta}{\partial\xi}\right)^2\right] - \sigma\left[\frac{\frac{2}{\tau_0}\frac{\partial^2\eta}{\partial\xi^2} + \frac{2}{\tau_0}\frac{\partial^2\eta}{\partial\zeta^2}}{\left[1 + \left(\frac{\partial\eta}{\partial\xi}\right)^2\right]^{\frac{3}{2}}}\right] = \frac{\sigma}{R_{stag}}$$

or:

$$\frac{U_s^2}{2}\left[1+\left(\frac{\partial\eta}{\partial\xi}\right)^2\right]-\left[\frac{\frac{\partial^2\eta}{\partial\xi^2}+\frac{\partial^2\eta}{\partial\zeta^2}}{\left[1+\left(\frac{\partial\eta}{\partial\xi}\right)^2\right]^{\frac{3}{2}}}\right]=\frac{\tau_0}{2R_{stag}}$$

or:

$$\frac{\partial^2\eta}{\partial\xi^2}+\frac{\partial^2\eta}{\partial\zeta^2}=\frac{1}{2}\left[U_s^2\left[1+\left(\frac{\partial\eta}{\partial\xi}\right)^2\right]-\frac{\tau_0}{R_{stag}}\right]\left[1+\left(\frac{\partial\eta}{\partial\xi}\right)^2\right]^{\frac{3}{2}} \tag{2-47}$$

From the continuity equation it was shown that:

$$(s\langle u\rangle)_x=-\frac{w_0}{2}\left(\frac{dA}{dz}\right)_x \tag{2-37}$$

In order to simplify the expression for U_s, it will be assumed that u_s is equal to $\langle u\rangle$. This removes any y-dependence on u, giving:

$$u_s=-\frac{w_0}{2s}\left(\frac{dA}{dz}\right)_x \tag{2-48}$$

and:

$$u_e=-\frac{w_0}{\tau_0}\left(\frac{dA_c}{dz}\right) \tag{2-49}$$

Therefore, if equations (2-48) and (2-49) are substituted into the definition of U_s, given in equation (2-46), it can be seen that:

$$U_s=\frac{\tau_0}{2s}\frac{\left(\frac{dA}{dz}\right)_x}{\frac{dA_c}{dz}}=\frac{1}{\eta}\frac{\left(\frac{dA}{dz}\right)_x}{\frac{dA_c}{dz}} \tag{2-50}$$

If it is assumed that the cross-sectional shape keeps a similar form for all z, then the definitions for the cross-sectional area of the sheet and the cross-sectional area of the edge cylinders may be scaled by r, or:

$$A=2r^2\int_0^{\frac{x}{r}}\left(\frac{s}{r}\right)d\left(\frac{x}{r}\right) \tag{2-51}$$

$$A_c = 2r^2 \int_0^1 \left(\frac{s}{r}\right) d\left(\frac{x}{r}\right) \tag{2-52}$$

Due to the assumption of the similar shapes and the scaling by r, the integrals in equations (2-51) and (2-52) can be assumed to be independent of z. This leaves the only z-dependence in the r in front of the integrals. The derivatives of these with respect to z may now be taken, giving:

$$\left(\frac{dA}{dz}\right)_x = 4r\frac{dr}{dz}\int_0^{\frac{x}{r}} \left(\frac{s}{r}\right) d\left(\frac{x}{r}\right) = \frac{2}{r}\frac{dr}{dz}A \tag{2-53}$$

$$\frac{dA_c}{dz} = 4r\frac{dr}{dz}\int_0^1 \left(\frac{s}{r}\right) d\left(\frac{x}{r}\right) = \frac{2}{r}\frac{dr}{dz}A_c \tag{2-54}$$

Substituting equations (2-53) and (2-54) into equation (2-50) gives:

$$U_s = \frac{1}{\eta}\frac{\frac{2}{r}\frac{dr}{dz}A}{\frac{2}{r}\frac{dr}{dz}A_c} = \frac{1}{\eta}\frac{A}{A_c} \tag{2-55}$$

Using the following dimensionless areas,

$$\overline{A} = \frac{2}{\tau_0^2}A;\ \overline{A}_c = \frac{2}{\tau_0^2}A_c \tag{2-56}$$

results in:

$$U_s = \frac{1}{\eta}\frac{\overline{A}}{\overline{A}_c} \tag{2-57}$$

Substituting this relation into equation (2-47) gives:

$$\frac{\partial^2\eta}{\partial\xi^2} + \frac{\partial^2\eta}{\partial\zeta^2} = \frac{1}{2}\left[\frac{1}{\eta^2}\left(\frac{\overline{A}}{\overline{A}_c}\right)^2\left[1 + \left(\frac{\partial\eta}{\partial\xi}\right)^2\right] - \frac{\tau_0}{R_{stag}}\right]\left[1 + \left(\frac{\partial\eta}{\partial\xi}\right)^2\right]^{\frac{3}{2}} \tag{2-58}$$

2.2.3 - Three Possible Simplified Solutions

The problem still remains to solve for η as a function of ξ and ζ. It would be easiest if all the z-dependence were removed. That is, to be able to solve for η as a function of ξ for any given $\overline{A}_c$. The only place where any z-dependence remains in this equation is in the $\partial^2\eta/\partial\zeta^2$ term. Three simplified solutions to this problem will be considered. In the first simplified solution, (i), this term will be neglected. In the second simplified solution, (ii), this term will be set equal to a constant. In the third simplified solution, (iii), this term is set proportional to the other second partial derivative term, that is,

$$\text{i)}\ \frac{\partial^2\eta}{\partial\zeta^2} = 0$$

$$\text{ii)}\ \frac{\partial^2\eta}{\partial\zeta^2} = Q = \text{constant}$$

$$\text{iii)}\ \frac{\partial^2\eta}{\partial\zeta^2} = \alpha\frac{\partial^2\eta}{\partial\xi^2}$$

Since, cases (i) and (ii) can be regarded as limiting cases of the more general case (iii), the solution for this case will be considered first.

Taking assumption (iii) and substituting into equation (2-58) yields:

$$\frac{d^2\eta}{d\xi^2} + \alpha\frac{d^2\eta}{d\xi^2} = \frac{1}{2}\left[\frac{1}{\eta^2}\left(\frac{\overline{A}}{\overline{A}_c}\right)^2\left[1+\left(\frac{d\eta}{d\xi}\right)^2\right] - \frac{\tau_0}{R_{stag}}\right]\left[1+\left(\frac{d\eta}{d\xi}\right)^2\right]^{\frac{3}{2}} \qquad (2\text{-}59)$$

This is a second order, non-linear, ordinary, differential equation which may be solved for η as a function of ξ for any $\overline{A}_c$. The boundary conditions on this equation are as follows:

$$1)\ \text{at } \xi = 0,\ \eta = 0 \text{ and } \frac{d\eta}{d\xi} \to \infty$$

$$2)\ \text{at } \xi = \bar{r},\ \eta = 1 \text{ and } \frac{d\eta}{d\xi} = 0$$

3) at $\xi = \bar{r}$, $\bar{A} = \bar{A}_c$

The solution can be found by using a fourth order Runge-Kutta technique. The algorithm uses what can be thought of as a shooting technique. τ_0/R_{stag} and α are free variables. Knowing $\bar{A}_c$, τ_0/R_{stag} and α are selected. Beginning at $\xi = 0$, where $\eta = 0$, the algorithm calculates η at $\Delta\xi$ and from that calculates η at $2\Delta\xi$ and so on. The program is allowed to shoot until η passes through a minimum. This point is $\bar{r}$. This insures a zero slope where the edge cylinder connects to the sheet. Thus the first part of boundary condition 1 and the second part of boundary condition 2 will always be satisfied. The next step in the routine is to insure that the proper τ_0/R_{stag} and α were selected.

First, the value of η at $\xi = \bar{r}$ is checked to see if it is equal to 1. If it is not, the value for α is changed and the algorithm is started again. This continues until the value of η at $\bar{r}$ is equal to 1. Second, the value of $\bar{A}$ at $\xi = \bar{r}$ is checked to see if it is equal to $\bar{A}_c$. If it is not, the value for τ_0/R_{stag} is changed and the algorithm is started over again. This most often results in α being changed again, but eventually both conditions are satisfied. This satisfies the first part of boundary condition 2 and boundary condition 3.

Due to the second part of boundary condition 1, the second point, $\eta(\Delta\xi)$, must be found by an analytic approximation. For small ξ, $\bar{A}$ is approximately equal to zero, and equation (2-59) reduces to:

$$\frac{d^2\eta}{d\xi^2} = -\frac{\tau_0\left[1+\left(\frac{d\eta}{d\xi}\right)^2\right]^{\frac{3}{2}}}{2R_{stag}(1+\alpha)} \qquad (2\text{-}60)$$

The solution to this equation is:

$$\eta = \left(\xi\left[\frac{4(1+\alpha)R_{stag}}{\tau_0} - \xi\right]\right)^{\frac{1}{2}} \qquad (2\text{-}61)$$

and

$$\frac{d\eta}{d\xi} = \frac{\left(\frac{2(1+\alpha)R_{stag}}{\tau_0} - \xi\right)}{\eta} \qquad (2\text{-}62)$$

The Fortran program SHAPE has been written to solve equation (2-59) using these boundary conditions and the approximations for small ξ. The listing of this program can be found in Appendix B. The results of running the SHAPE program for a number of $\bar{A}_c$'s are shown graphically in Figure 2-6. Figure 2-7 shows that there are only specific values of α and τ_0/R_{stag} that can exist for any given $\bar{A}_c$. These two quantities quickly diverge as $\bar{A}_c$ approaches 0. For this reason, results for $\bar{A}_c$'s less then 40 were unable to be obtained. One interesting note is that if assumption (i) had been used it would have been equivalent to setting α equal to 0 in this solution. As can be seen from this graph, the only $\bar{A}_c$ at which the boundary conditions could be satisfied had this term been neglected is approximately 454. For this reason it is apparent that assumption (i) would have been invalid. Figure 2-8 shows how the quantities η_{max} and $\bar{r}$ vary with $\bar{A}_c$. η_{max} is the largest value η reaches in the cross-sectional shape and represents half of the maximum thickness of the cylinder. Figure 2-9 shows the ellipticity of the end cylinder. This is particularly

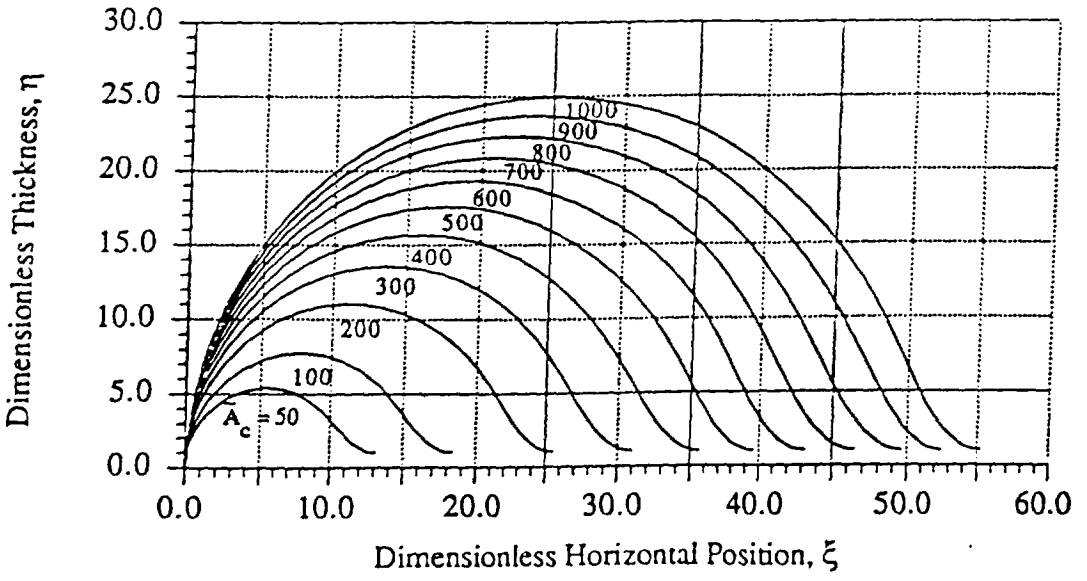

Figure 2-6 Cross-Sectional Shape of the Edge Cylinder for Case (iii)

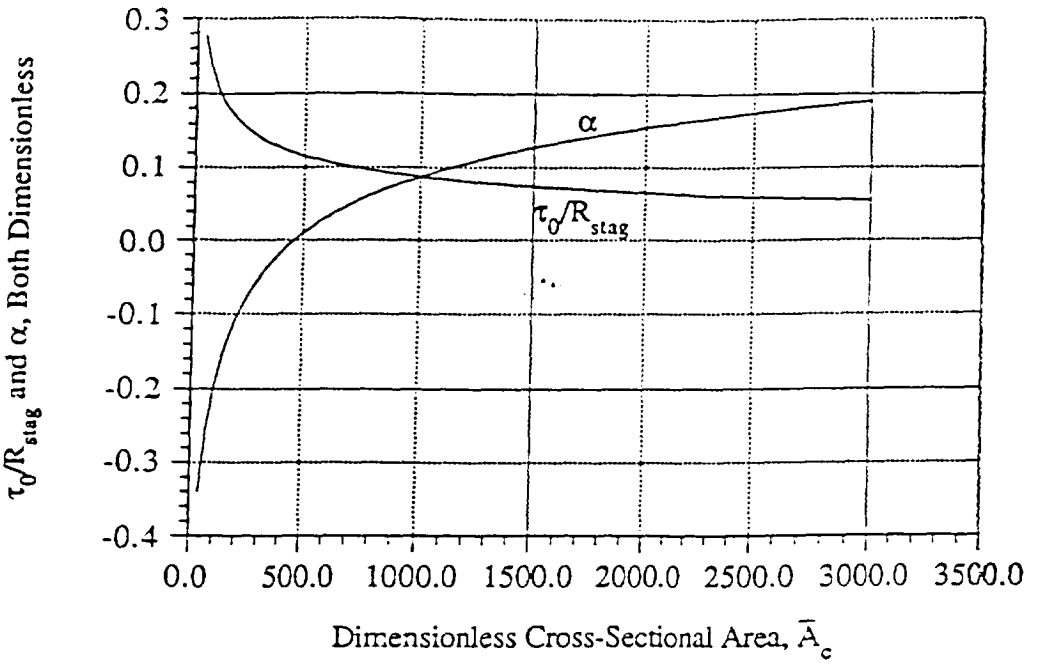

Figure 2-7 τ_0/R_{stag} and α vs. Dimensionless Cross-Sectional Area for Case (iii)

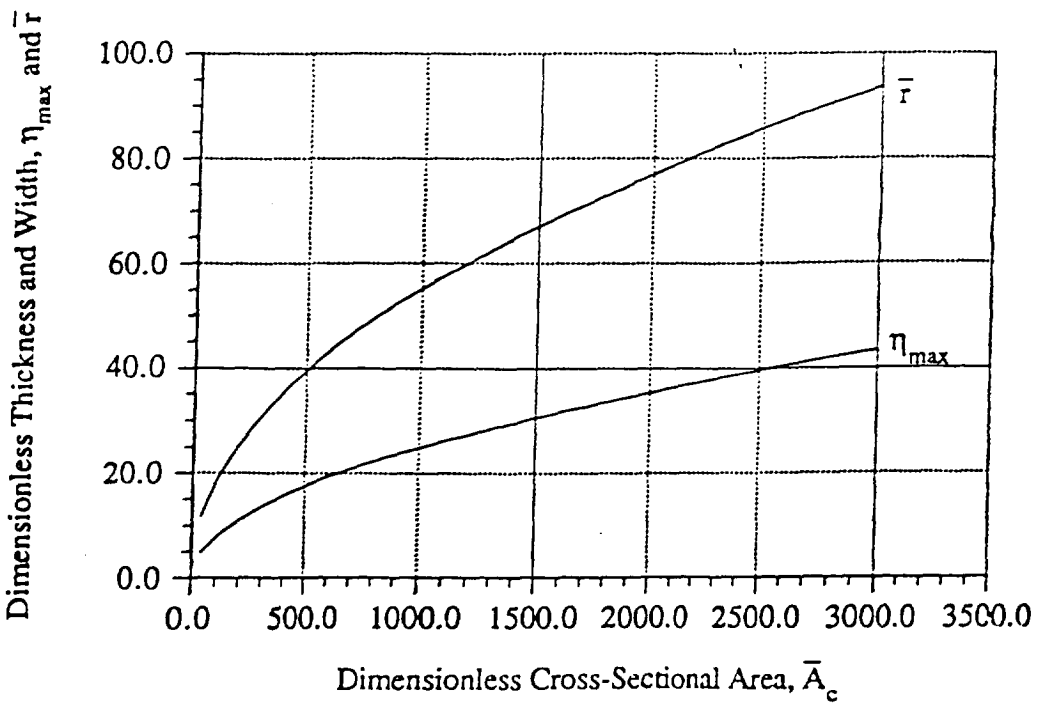

Figure 2-8 η_{max} and $\bar{r}$ vs. Dimensionless Cross-Sectional Area for Case (iii)

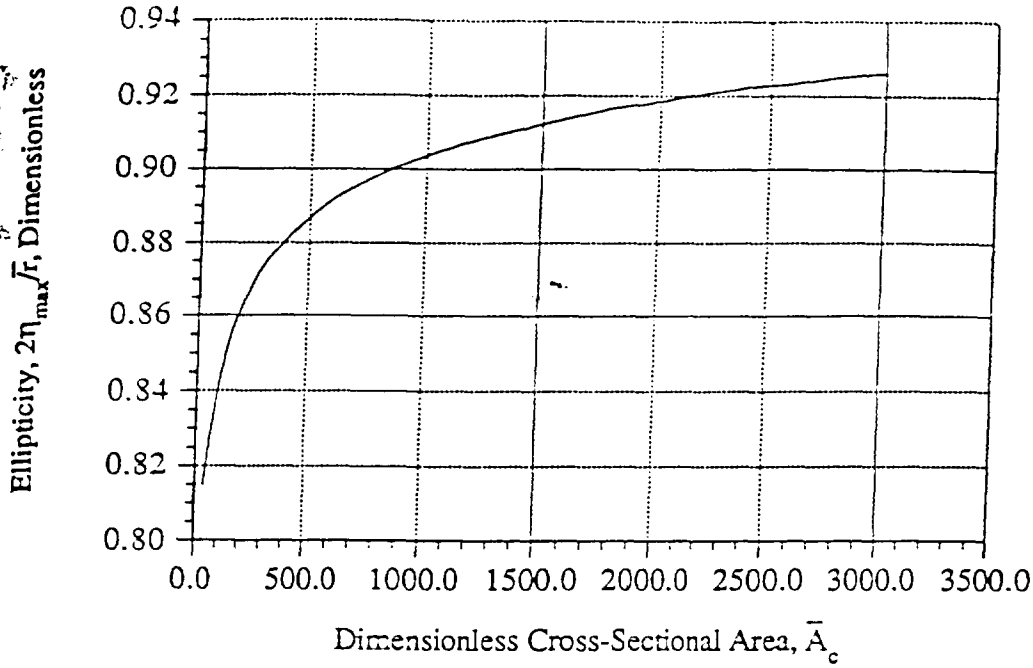

Figure 2-9 Ellipticity vs. Dimensionless Cross-Sectional Area for Case (iii)

interesting in that it shows for small areas the cylinder is wider then it is thick, but for larger areas the cylinder approaches a more circular cross-section, which would have been intuitively expected.

Taking assumption (ii) and substituting into equation (2-58) yields:

$$\frac{d^2\eta}{d\xi^2} = \frac{1}{2}\left[\frac{1}{\eta^2}\left(\frac{\bar{A}}{\bar{A}_c}\right)^2\left[1+\left(\frac{d\eta}{d\xi}\right)^2\right] - \frac{\tau_0}{R_{stag}}\right]\left[1+\left(\frac{d\eta}{d\xi}\right)^2\right]^{\frac{3}{2}} - Q \qquad (2\text{-}63)$$

This equation is solved similarly to the previous one. The method is the same and the boundary conditions are the same, the only difference is the two free constants are now τ_0/R_{stag} and Q. The second point $\eta(\Delta\xi)$ still has to be found using an analytic approximation. If $\bar{A}$ and Q are set equal to zero in equation (2-63) it yields:

$$\frac{d^2\eta}{d\xi^2} = -\frac{\tau_0}{2R_{stag}}\left[1+\left(\frac{d\eta}{d\xi}\right)^2\right]^{\frac{3}{2}} \tag{2-64}$$

The solution to this equation is:

$$\eta = \left(\xi\left[\frac{4R_{stag}}{\tau_0} - \xi\right]\right)^{\frac{1}{2}} \tag{2-65}$$

and

$$\frac{d\eta}{d\xi} = \frac{\left(\frac{2R_{stag}}{\tau_0} - \xi\right)}{\eta} \tag{2-66}$$

The Fortran program SHAPE2 has been written to solve equation (2-63) with the

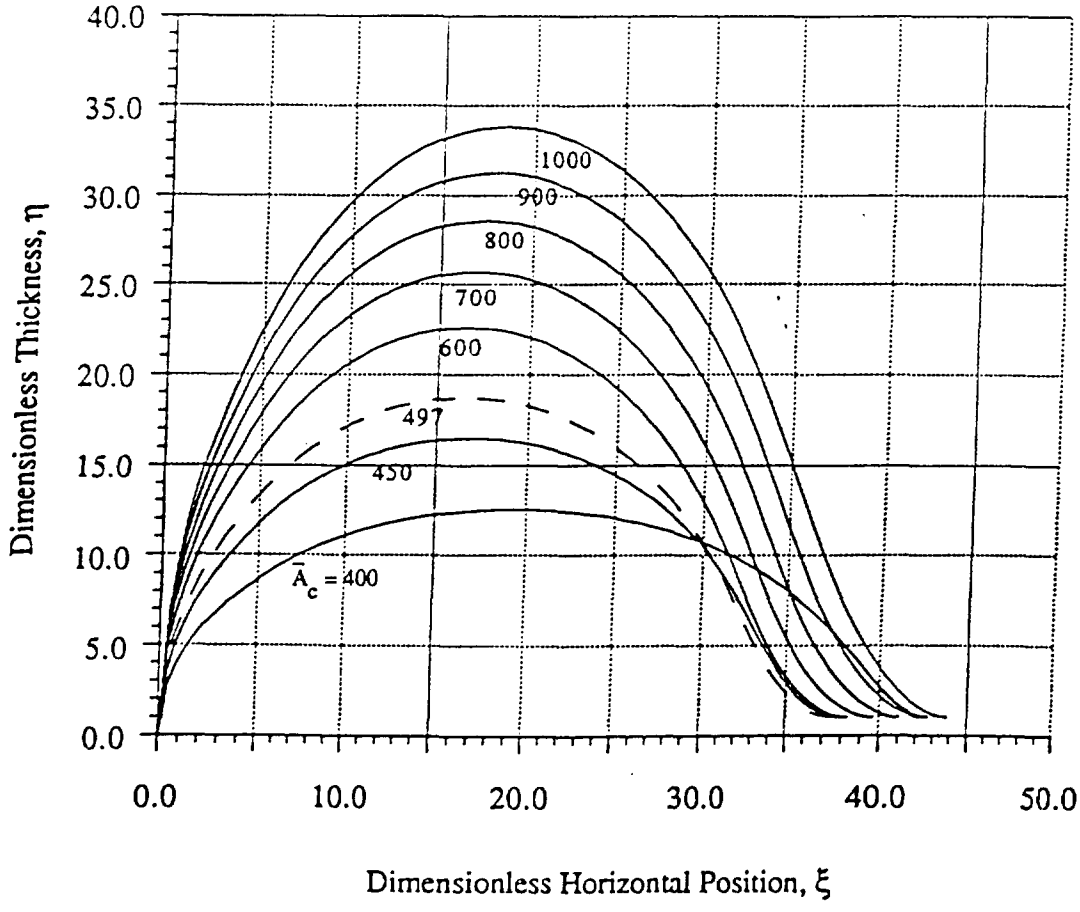

Figure 2-10 Cross-Sectional Shape of the Edge Cylinder for Case (ii)

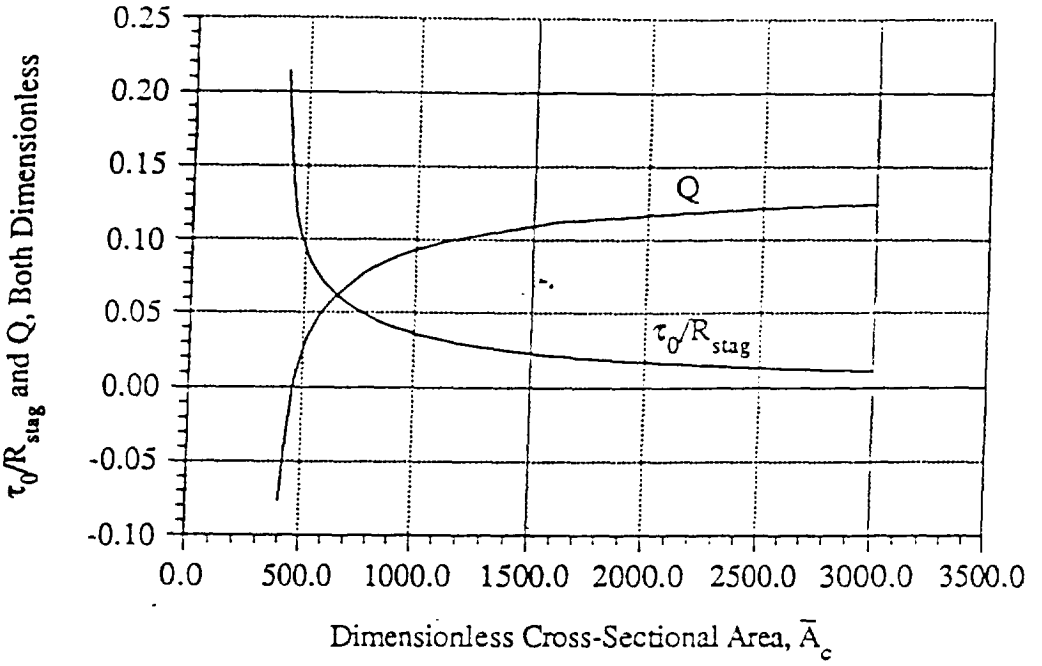

Figure 2-11 τ_0/R_{stag} and Q vs. Dimensionless Cross-Sectional Area for Case (ii)

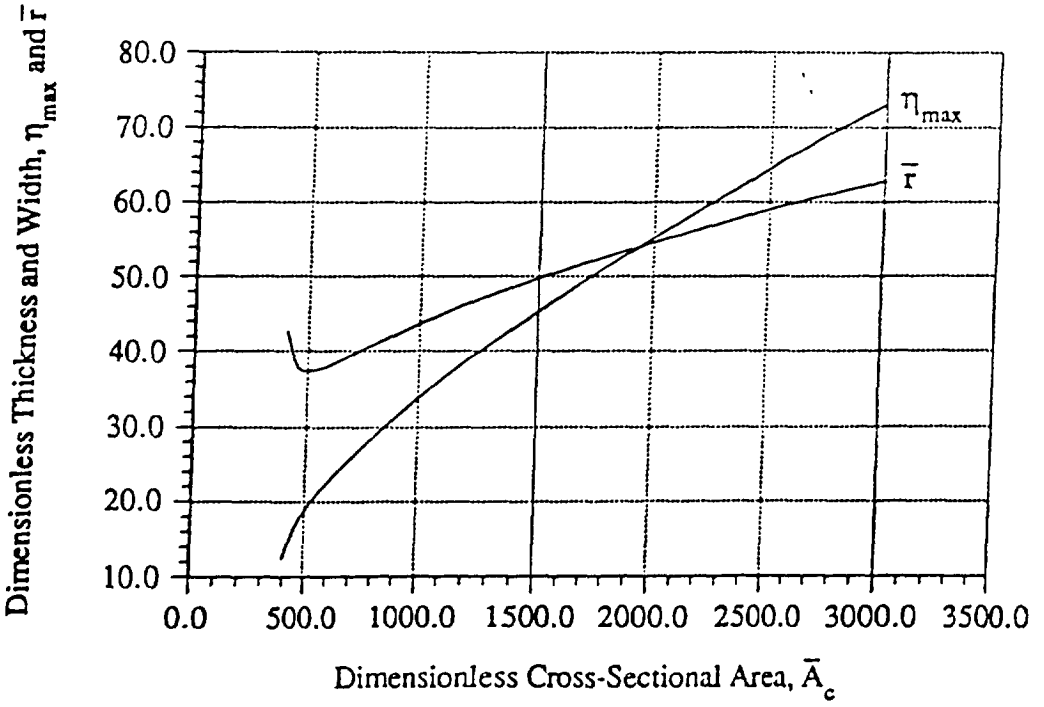

Figure 2-12 η_{max} and $\bar{r}$ vs. Dimensionless Cross-Sectional Area for Case (ii)

same boundary conditions as before and these approximations for small ξ. The listing of this program is also appended. Figure 2-10 shows the results of SHAPE2 when it was ran for a number of $\bar{A}_c$'s. Figure 2-11 shows there is only one specific τ_0/R_{stag} and Q for any given $\bar{A}_c$. This is also in agreement with the previous solution in that if assumption (i) was used the only value of $\bar{A}_c$ where the boundary conditions could have been satisfied was 454. Figure 2-12 shows how η_{max} and $\bar{r}$ vary with $\bar{A}_c$. This is quite peculiar where it shows that for $\bar{A}_c$'s less then 497 a decrease in area actually produces an increase in $\bar{r}$. This is definitely not to be expected. The computer solution became quite unstable for small values of $\bar{A}_c$, for this reason, no values were obtained for $\bar{A}_c$'s less then 400. Figure 2-13 shows the ellipticity using assumption (ii). This is quite unexpected, for $\bar{A}_c$'s greater

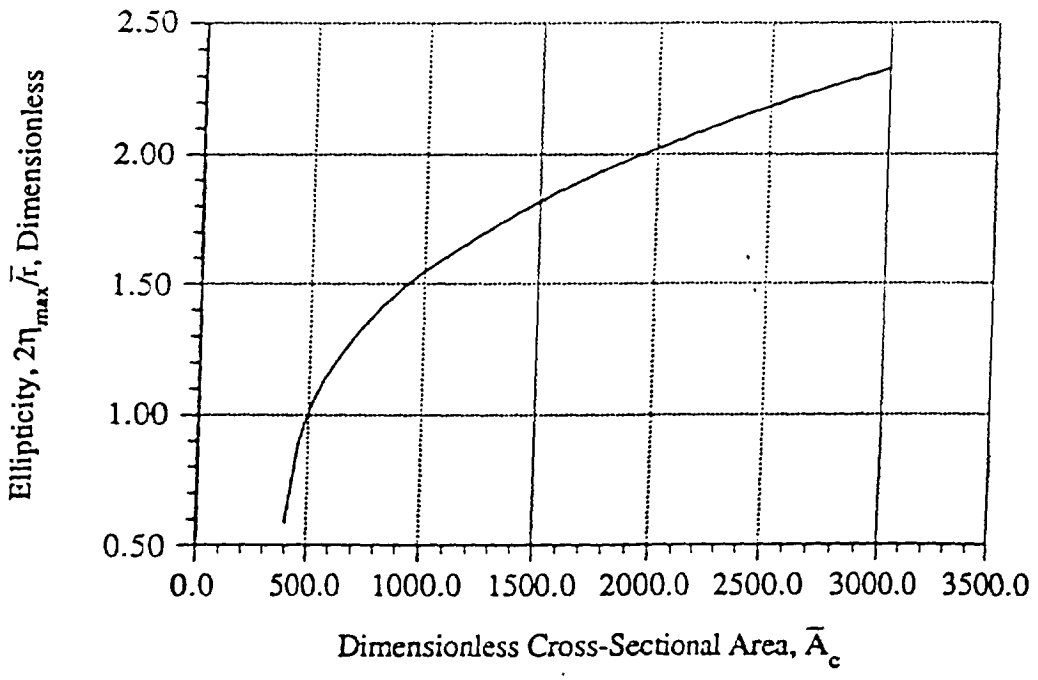

Figure 2-13 Ellipticity vs. Dimensionless Cross-Sectional Area for Case (ii)

then 497 the cylinder becomes thicker than it is wide. This is very apparent in Figure 2-10 where the curve corresponding to an $\bar{A}_c$ of 497 is dashed and the curves below it have a

large $\bar{r}$. This is very different then case (iii) where the cylinder approached a circular shape for large $\bar{A}_c$'s. For these reasons assumption (ii) will have to be discarded and assumption (iii) accepted as the best of the three simplified solutions.

With assumption (iii) being accepted as a physically possible solution, all that remains is to determine $\bar{A}_c$ and run the SHAPE program for this value. It was shown earlier that:

$$\bar{A}_c = \frac{2}{\tau_0^2} A_c \tag{2-56}$$

but,

$$A_c = \tau_0 z \sqrt{\frac{2}{We}} \tag{2-40}$$

Therefore:

$$\bar{A}_c = \frac{2z}{\tau_0} \sqrt{\frac{2}{We}} \tag{2-67}$$

From Chapter 2, Section 1 it was shown that:

$$\frac{L}{W_0} = \sqrt{\frac{We}{8}} \tag{2-19}$$

Substituting equation (2-19) into equation (2-67) gives:

$$\bar{A}_c = \frac{W_0 z}{\tau_0 L} \tag{2-63}$$

With this expression, all that has to be known is the dimensions of the slit, the length of the sheet, and how far down the sheet the shape is desired to be known to calculate $\bar{A}_c$. Once this is known, the program SHAPE is ran and the output describes the theoretical cross-sectional shape.

Chapter 3
Stability Analysis

The focus of this chapter is to analytically predict the stability of a non-planer, thin liquid sheet. It has already been shown by Geoffrey Taylor [1] that a perfectly planer liquid sheet is completely stable. It has also been shown by Rayleigh [4] that a cylindrical jet is unstable to an asymmetric disturbance. Unlike Taylor's work, the sheet in this study is not perfectly planer and does not have a zero velocity throughout in the transverse direction. The sheet has curvature, particularly in the edge cylinders and also in the sheet itself due to slit defects. With this in mind, this particular analysis may be considered a combination of Taylor's and Rayleigh's work.

By neglecting gravity the velocity field to be considered is the following:

$$\mathbf{V} \Rightarrow u(x,y,z),\ v(x,y,z),\ \dot{w}_0$$

Without loss of generality a Galilean transformation may be made to reduce the z-direction velocity to rest, leaving:

$$\mathbf{V} = u(x,y,t),\ v(x,y,t);\ w = 0$$

Assuming an incompressible fluid, the continuity equation may be written for this flow field as:

$$\frac{\partial u}{\partial x} + \frac{\partial v}{\partial y} = 0$$

Assuming irrotational flow, it may be written that:

$$\frac{\partial u}{\partial y} - \frac{\partial v}{\partial x} = 0$$

Introducing a velocity potential to satisfy the irrotational assumption,

$$u = \frac{\partial \phi}{\partial x},\ v = \frac{\partial \phi}{\partial y} \tag{3-1}$$

and substituting it into the continuity equation yields the two-dimensional Laplace equation.

$$\frac{\partial^2 \phi}{\partial x^2} + \frac{\partial^2 \phi}{\partial y^2} = 0 \tag{3-2}$$

The first boundary condition that the flow field must satisfy is the kinematic condition: that the fluid particle's y-direction velocity must be equal to the motion of the free surface, or mathematically since s = s(x,t):

$$\frac{ds}{dt} = \frac{\partial s}{\partial t} + \frac{\partial s}{\partial x}\left(\frac{dx}{dt}\right)_s$$

but,

$$\frac{ds}{dt} = v_s = \left(\frac{\partial \phi}{\partial y}\right)_s$$

$$\left(\frac{dx}{dt}\right)_s = u_s = \left(\frac{\partial \phi}{\partial x}\right)_s$$

therefore:

$$\left(\frac{\partial \phi}{\partial y}\right)_s = \frac{\partial s}{\partial t} + \frac{\partial s}{\partial x}\left(\frac{\partial \phi}{\partial x}\right)_s \tag{3-3}$$

The second boundary condition is obtained by applying the unsteady Bernoulli equation including surface tension.

$$\left(\frac{\partial \phi}{\partial t}\right)_s + \frac{1}{2}\left(u_s^2 + v_s^2\right) - \frac{\sigma}{\rho}\frac{\dfrac{\partial^2 s}{\partial x^2}}{\left(1 + \left(\dfrac{\partial s}{\partial x}\right)^2\right)^{3/2}} = \text{constant}$$

Substituting for u_s and v_s gives:

$$\left(\frac{\partial \phi}{\partial t}\right)_s + \frac{1}{2}\left(\left(\frac{\partial \phi}{\partial x}\right)_s^2 + \left(\frac{\partial \phi}{\partial y}\right)_s^2\right) - \frac{\sigma}{\rho}\frac{\dfrac{\partial^2 s}{\partial x^2}}{\left(1 + \left(\dfrac{\partial s}{\partial x}\right)^2\right)^{3/2}} = \text{constant} \tag{3-4}$$

The flow on the sheet surface must satisfy equation (3-2) and the boundary conditions, equations (3-3) and (3-4).

If ϕ_0 and s_0 are the solutions to these equations, a small perturbation or disturbance $\Delta\phi$ and Δs may be added to these solutions as follows:

$$\phi = \phi_0(x,y) + \Delta\phi(x,y,t) \tag{3-5}$$

$$s = s_0(x) + \Delta s(x,t) \tag{3-6}$$

These values for ϕ and s may be substituted into equation (3-2) to obtain the disturbance equation.

$$\frac{\partial^2}{\partial x^2}(\phi_0 + \Delta\phi) + \frac{\partial^2}{\partial y^2}(\phi_0 + \Delta\phi) = 0$$

$$\frac{\partial^2\phi_0}{\partial x^2} + \frac{\partial^2\Delta\phi}{\partial x^2} + \frac{\partial^2\phi_0}{\partial y^2} + \frac{\partial^2\Delta\phi}{\partial y^2} = 0$$

Removing the terms that are identically zero by equation (3-2) leaves:

$$\frac{\partial^2\Delta\phi}{\partial x^2} + \frac{\partial^2\Delta\phi}{\partial y^2} = 0 \tag{3-7}$$

Equations (3-5) and (3-6) may also be substituted into the boundary conditions. Substituting equations (3-5) and (3-6) into equation (3-3) yields the following.

$$\frac{\partial}{\partial y}(\phi_0 + \Delta\phi)_s = \frac{\partial}{\partial t}(s_0 + \Delta s) + \frac{\partial}{\partial x}(s_0 + \Delta s)\frac{\partial}{\partial x}(\phi_0 + \Delta\phi)_s$$

or,

$$\left(\frac{\partial\phi_0}{\partial y}\right)_s + \left(\frac{\partial\Delta\phi}{\partial y}\right)_s = \frac{\partial s_0}{\partial t} + \frac{\partial\Delta s}{\partial t} + \left[\frac{\partial s_0}{\partial x}\left(\frac{\partial\phi_0}{\partial x}\right)_s + \frac{\partial\Delta s}{\partial x}\left(\frac{\partial\phi_0}{\partial x}\right)_s + \frac{\partial s_0}{\partial x}\left(\frac{\partial\Delta\phi}{\partial x}\right)_s + \frac{\partial\Delta s}{\partial x}\left(\frac{\partial\Delta\phi}{\partial x}\right)_s\right]$$

The terms that are identically zero by equation (3-3) can be removed from the above equation. By the assumption that $\Delta\phi$ and Δs are small, the last term in the above equation may be neglected, thus resulting in a linear equation in $\Delta\phi$ and Δs.

$$\left(\frac{\partial \Delta\phi}{\partial y}\right)_s = \frac{\partial \Delta s}{\partial t} + \frac{\partial \Delta s}{\partial x}\left(\frac{\partial \phi_0}{\partial x}\right)_s + \frac{\partial s_0}{\partial x}\left(\frac{\partial \Delta\phi}{\partial x}\right)_s \qquad (3\text{-}8)$$

Substituting equations (3-5) and (3-6) into equation (3-4) yields the following.

$$\frac{\partial}{\partial t}(\phi_0 + \Delta\phi)_s + \frac{1}{2}\left[\left(\frac{\partial}{\partial x}(\phi_0 + \Delta\phi)_s\right)^2 + \left(\frac{\partial}{\partial y}(\phi_0 + \Delta\phi)_s\right)^2\right] - \frac{\sigma}{\rho}\frac{\frac{\partial^2}{\partial x^2}(s_0 + \Delta s)}{\left(1 + \left(\frac{\partial}{\partial x}(s_0 + \Delta s)\right)^2\right)^{3/2}} = \text{constant}$$

or:

$$\left(\frac{\partial \phi_0}{\partial t}\right)_s + \left(\frac{\partial \Delta\phi}{\partial t}\right)_s + \frac{1}{2}\left(\left(\frac{\partial \phi_0}{\partial x}\right)_s^2 + 2\left(\frac{\partial \phi_0}{\partial x}\right)_s\left(\frac{\partial \Delta\phi}{\partial x}\right)_s + \left(\frac{\partial \Delta\phi}{\partial x}\right)_s^2 + \left(\frac{\partial \phi_0}{\partial y}\right)_s^2 + 2\left(\frac{\partial \phi_0}{\partial y}\right)_s\left(\frac{\partial \Delta\phi}{\partial y}\right)_s + \left(\frac{\partial \Delta\phi}{\partial y}\right)_s^2\right)$$

$$-\frac{\sigma}{\rho}\frac{\frac{\partial^2 s_0}{\partial x^2} + \frac{\partial^2 \Delta s}{\partial x^2}}{\left(1 + \left(\frac{\partial s_0}{\partial x}\right)^2 + 2\frac{\partial s_0}{\partial x}\frac{\partial \Delta s}{\partial x} + \left(\frac{\partial \Delta s}{\partial x}\right)^2\right)^{3/2}} = \text{constant}$$

Since $\Delta\phi$ and Δs are small the non-linear terms in $\Delta\phi$ and Δs may be neglected, resulting in:

$$\left(\frac{\partial \phi_0}{\partial t}\right)_s + \left(\frac{\partial \Delta\phi}{\partial t}\right)_s + \frac{1}{2}\left(\left(\frac{\partial \phi_0}{\partial x}\right)_s^2 + 2\left(\frac{\partial \phi_0}{\partial x}\right)_s\left(\frac{\partial \Delta\phi}{\partial x}\right)_s + \left(\frac{\partial \phi_0}{\partial y}\right)_s^2 + 2\left(\frac{\partial \phi_0}{\partial y}\right)_s\left(\frac{\partial \Delta\phi}{\partial y}\right)_s\right)$$

$$-\frac{\sigma}{\rho}\frac{\frac{\partial^2 s_0}{\partial x^2} + \frac{\partial^2 \Delta s}{\partial x^2}}{\left(1 + \left(\frac{\partial s_0}{\partial x}\right)^2\right)^{3/2}} = \text{constant}$$

Removing the terms that are identically zero by equation (3-4) results in:

$$\left(\frac{\partial \Delta\phi}{\partial t}\right)_s + \left(\frac{\partial \phi_0}{\partial x}\right)_s\left(\frac{\partial \Delta\phi}{\partial x}\right)_s + \left(\frac{\partial \phi_0}{\partial y}\right)_s\left(\frac{\partial \Delta\phi}{\partial y}\right)_s - \frac{\sigma}{\rho}\frac{\frac{\partial^2 \Delta s}{\partial x^2}}{\left(1 + \left(\frac{\partial s_0}{\partial x}\right)^2\right)^{3/2}} = 0 \qquad (3\text{-}9)$$

Next, assume a wavelike form in x and t for $\Delta\phi$ and Δs as:

$$\Delta\phi = \hat{\phi}(y)e^{i(kx - \omega t)} \tag{3-10}$$

$$\Delta s = \hat{s}e^{i(kx - \omega t)} \tag{3-11}$$

where ω is the frequency and k is given by the following relation:

$$k = \frac{2\pi}{\lambda} \tag{3-12}$$

where λ is the wavelength. These wavelike forms may be substituted into the disturbance equation, equation (3-7), and into the boundary conditions, equations (3-8) and (3-9). The resulting equations may then be solved for ω. If there is a positive imaginary part to ω then any initially small disturbance will grow exponentially with time causing the solution to be unstable.

These wavelike forms can be substituted into equation (3-7), yielding:

$$\frac{\partial^2}{\partial x^2}\left(\hat{\phi}e^{i(kx - \omega t)}\right) + \frac{\partial^2}{\partial y^2}\left(\hat{\phi}e^{i(kx - \omega t)}\right) = 0$$

$$\hat{\phi}(ik)^2 e^{i(kx - \omega t)} + e^{i(kx - \omega t)}\frac{d^2\hat{\phi}}{dy^2} = 0$$

or,

$$\frac{d^2\hat{\phi}}{dy^2} - k^2\hat{\phi} = 0 \tag{3-13}$$

The solution to equation (3-13) is as follows:

$$\hat{\phi} = c_1\sinh(ky) + c_2\cosh(ky) \tag{3-14}$$

where c_1 and c_2 are constants. Therefore, substituting equations (3-14) and (3-10) into equation (3-5) gives:

$$\phi = \phi_0 + (c_1\sinh(ky) + c_2\cosh(ky))e^{i(kx - \omega t)} \tag{3-15}$$

Since every wavelike disturbance can be considered as a combination of a symmetric and an asymmetric wave, these are the only two waves that need to be

considered. In the symmetric case, the y-velocity on the back surface of the sheet is the opposite of that on the front surface. In the asymmetric case, the y-velocity on the back surface of the sheet is equal to that on the front. These two cases are shown in Figure 3-1. The boundary conditions for these two cases are as follows.

1) Symmetric Case

$$v_s = - v_{-s}$$

$$\left(\frac{\partial \phi}{\partial y}\right)_s = -\left(\frac{\partial \phi}{\partial y}\right)_{-s} \tag{3-16}$$

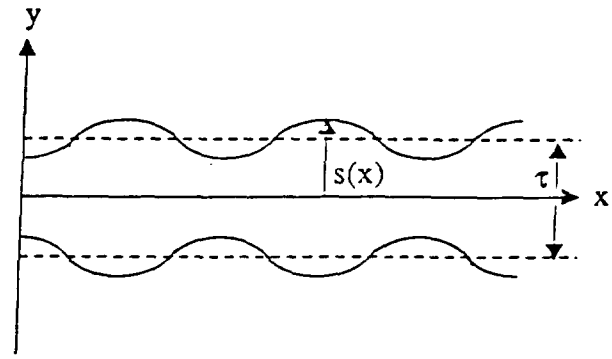

Symmetric Case

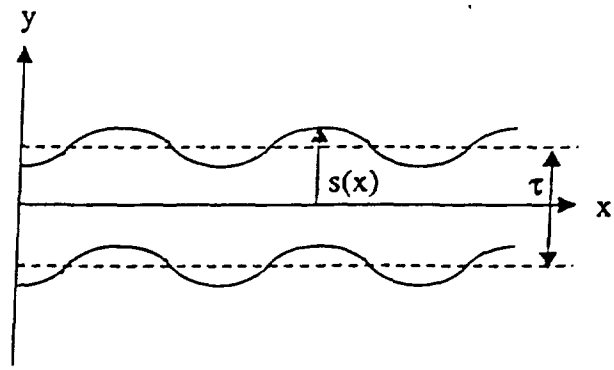

Asymmetric Case

Figure 3-1 Schematic of the Symmetric and Asymmetric Waves

2) Asymmetric Case

$$v_s = v_{-s}$$

$$\left(\frac{\partial\phi}{\partial y}\right)_s = \left(\frac{\partial\phi}{\partial y}\right)_{-s} \qquad (3\text{-}17)$$

For case 1, the symmetric case, boundary condition (3-16) can be applied to equation (3-15), giving:

$$\left(\frac{\partial\phi_0}{\partial y}\right)_s + (c_1\cosh(ks) + c_2\sinh(ks))e^{i(kx - \omega t)} = -\left(\frac{\partial\phi_0}{\partial y}\right)_{-s} - (c_1\cosh(-ks) + c_2\sinh(-ks))e^{i(kx - \omega t)}$$

The first terms on both sides of this equation are equal from equation (3-16). Rewriting using trigonometric identities gives:

$$(c_1\cosh(ks) + c_2\sinh(ks))e^{i(kx - \omega t)} = -(c_1\cosh(ks) - c_2\sinh(ks))e^{i(kx - \omega t)}$$

Simplifying yields:

$$c_1 = -c_1$$

Therefore, for the symmetric case, c_1 must be equal to zero. Now if c_2 is set equal to A_{sy}, the amplitude can be written as:

$$\hat{\phi} = A_{sy}\cosh(ky) \qquad \text{Symmetric Case} \qquad (3\text{-}18)$$

For case 2, the asymmetric case, boundary condition (3-17) can be applied to equation (3-15), yielding:

$$\left(\frac{\partial\phi_0}{\partial y}\right)_s + (c_1\cosh(ks) + c_2\sinh(ks))e^{i(kx - \omega t)} = \left(\frac{\partial\phi_0}{\partial y}\right)_{-s} + (c_1\cosh(-ks) + c_2\sinh(-ks))e^{i(kx - \omega t)}$$

According to boundary condition (3-17) the first term on both sides of this equation are equal. Rewriting with the use of trigonometric identities gives:

$$(c_1\cosh(ks) + c_2\sinh(ks))e^{i(kx - \omega t)} = (c_1\cosh(ks) - c_2\sinh(ks))e^{i(kx - \omega t)}$$

Simplifying gives:

$$c_2 = -c_2$$

Therefore, for the asymmetric case, c_2 must be equal to zero and if c_1 is set equal to A_{asy}, it yields:

$$\hat{\phi} = A_{asy}\sinh(ky) \qquad \text{Asymmetric Case} \qquad (3\text{-}19)$$

The wavelike forms may also be applied to the boundary conditions. If equations (3-10) and (3-11) are applied to equation (3-8) it gives:

$$e^{i(kx - \omega t)}\left(\frac{\partial\hat{\phi}}{\partial y}\right)_s = \hat{s}e^{i(kx - \omega t)}(-i\omega) + \hat{s}e^{i(kx - \omega t)}(ik)\left(\frac{\partial\phi_0}{\partial x}\right)_s + \frac{\partial s_0}{\partial x}\hat{\phi}_s e^{i(kx - \omega t)}(ik)$$

Dividing out the exponentials and multiplying by i gives:

$$i\left(\frac{\partial\hat{\phi}}{\partial y}\right)_s = \hat{s}\omega - \hat{s}k\left(\frac{\partial\phi_0}{\partial x}\right)_s - \frac{\partial s_0}{\partial x}\hat{\phi}_s k \qquad (3\text{-}20)$$

If equations (3-10) and (3-11) are applied to equation (3-9) it yields:

$$\hat{\phi}_s e^{i(kx - \omega t)}(-i\omega) + \left(\frac{\partial\phi_0}{\partial x}\right)_s\hat{\phi}_s e^{i(kx - \omega t)}(ik) + \left(\frac{\partial\phi_0}{\partial y}\right)_s\left(\frac{\partial\hat{\phi}}{\partial y}\right)_s e^{i(kx - \omega t)} - \frac{\sigma}{\rho}\frac{\hat{s}e^{i(kx - \omega t)}(ik)^2}{\left(1 + \left(\frac{\partial s_0}{\partial x}\right)^2\right)^{3/2}} = 0$$

Simplifying yields:

$$-\hat{\phi}_s i\omega + \left(\frac{\partial\phi_0}{\partial x}\right)_s\hat{\phi}_s ik + \left(\frac{\partial\phi_0}{\partial y}\right)_s\left(\frac{\partial\hat{\phi}}{\partial y}\right)_s + \frac{\sigma}{\rho}\frac{\hat{s}k^2}{\left(1 + \left(\frac{\partial s_0}{\partial x}\right)^2\right)^{3/2}} = 0 \qquad (3\text{-}21)$$

Simultaneously substituting equation (3-18), for the symmetric case, into both boundary conditions, equations (3-20) and (3-21), at y equal to s_0 yields:

$$ikA_{sy}\sinh(ks_0) = \hat{s}\omega - u_{s,0}\hat{s}k - \left(\frac{\partial s_0}{\partial x}\right)kA_{sy}\cosh(ks_0) \qquad (3\text{-}22)$$

and

$$-i\omega A_{sy}\cosh(ks_0) + iku_{s,0}A_{sy}\cosh(ks_0) + kv_{s,0}A_{sy}\sinh(ks_0) + \frac{\sigma}{\rho}\frac{\hat{s}k^2}{\left(1 + \left(\frac{\partial s_0}{\partial x}\right)^2\right)^{3/2}} \qquad (3\text{-}23)$$

Solving equation (3-22) for $\hat{s}$ and substituting into equation (3-23) yields:

$$\cosh(ks_0)(-i\omega A_{sy} + iku_{s,0}A_{sy}) + kv_{s,0}A_{sy}\sinh(ks_0)$$

$$+\frac{\sigma}{\rho}\frac{\left(ikA_{sy}\sinh(ks_0) + \frac{\partial s_0}{\partial x}kA_{sy}\cosh(ks_0)\right)k^2}{(\omega - ku_{s,0})\left(1 + \left(\frac{\partial s_0}{\partial x}\right)^2\right)^{3/2}} = 0$$

Dividing by $A_{sy}\cosh(ks_0)$ yields:

$$-i(\omega - ku_{s,0}) + kv_{s,0}\tanh(ks_0) + \frac{\sigma}{\rho}\frac{k^3\left(i\tanh(ks_0) + \frac{\partial s_0}{\partial x}\right)}{(\omega - ku_{s,0})\left(1 + \left(\frac{\partial s_0}{\partial x}\right)^2\right)^{3/2}} = 0$$

Define:

$$\omega' = \omega - ku_{s,0} \tag{3-24}$$

$$\rho' = \rho\left(1 + \left(\frac{\partial s_0}{\partial x}\right)^2\right)^{3/2} \tag{3-25}$$

Therefore:

$$-i\omega' + kv_{s,0}\tanh(ks_0) + \frac{\sigma k^3}{\rho'\omega'}\left(i\tanh(ks_0) + \frac{\partial s_0}{\partial x}\right) = 0$$

Multiplying by $\omega' i$ gives:

$$(\omega')^2 + ikv_{s,0}\tanh(ks_0)\omega' + \frac{k^3\sigma}{\rho'}\left(i\frac{\partial s_0}{\partial x} - \tanh(ks_0)\right) = 0 \quad \text{Symmetric Case} \tag{3-26}$$

Substituting equation (3-19), for the asymmetric case, into both boundary conditions, equations (3-20) and (3-21), at y equal to s_0 yields:

$$ikA_{asy}\cosh(ks_0) = \hat{s}\omega - u_{s,0}\hat{s}k - \left(\frac{\partial s_0}{\partial x}\right)kA_{asy}\sinh(ks_0) \tag{3-27}$$

and

$$-i\omega A_{asy}\sinh(ks_0) + iku_{s,0}A_{asy}\sinh(ks_0) + kv_{s,0}A_{asy}\cosh(ks_0) + \frac{\sigma}{\rho}\frac{\hat{s}k^2}{\left(1 + \left(\frac{\partial s_0}{\partial x}\right)^2\right)^{3/2}} \tag{3-28}$$

Solving equation (3-27) for $\hat{s}$ and substituting into equation (3-28) yields:

$$\sinh(ks_0)(-i\omega A_{asy} + iku_{s,0}A_{asy}) + kv_{s,0}A_{asy}\cosh(ks_0)$$

$$+\frac{\sigma}{\rho}\frac{\left(ikA_{asy}\cosh(ks_0) + \frac{\partial s_0}{\partial x}kA_{asy}\sinh(ks_0)\right)k^2}{(\omega - ku_{s,0})\left(1 + \left(\frac{\partial s_0}{\partial x}\right)^2\right)^{3/2}} = 0$$

Dividing by $A_{asy}\sinh(ks_0)$ yields:

$$-i(\omega - ku_{s,0}) + kv_{s,0}\coth(ks_0) + \frac{\sigma}{\rho}\frac{k^3\left(i\coth(ks_0) + \frac{\partial s_0}{\partial x}\right)}{(\omega - ku_{s,0})\left(1 + \left(\frac{\partial s_0}{\partial x}\right)^2\right)^{3/2}} = 0$$

Employing the above defined variables, yields:

$$-i\omega' + kv_{s,0}\coth(ks_0) + \frac{\sigma k^3}{\rho'\omega'}\left(i\coth(ks_0) + \frac{\partial s_0}{\partial x}\right) = 0$$

Multiplying by $\omega' i$ gives:

$$(\omega')^2 + ikv_{s,0}\coth(ks_0)\omega' + \frac{k^3\sigma}{\rho'}\left(i\frac{\partial s_0}{\partial x} - \coth(ks_0)\right) = 0 \qquad \text{Asymmetric Case (3-29)}$$

Thus we have two relations, equation (3-26) and equation (3-29), that describe the behavior of the complex frequency for a symmetric and an asymmetric wave. If either of the two roots for ω have positive imaginary parts an unstable solution for the boundary, s, will exist.

One case of interest will be that of the thin, flat section of the sheet. This is the same as the problem first solved by Taylor [1]. In the flat thin sheet case:

$$v_{s,0} = u_{s,0} = 0$$

$$s_0 = \frac{\pi}{2} \text{ and } \frac{\partial s_0}{\partial x} = 0$$

Therefore, equations (3-24) and (3-25) reduce to:

$$\omega' = \omega - k u_{s,0} = \omega$$

$$\rho' = \rho\left(1 + \left(\frac{\partial s_0}{\partial x}\right)^2\right)^{3/2} = \rho$$

Therefore, equations (3-26) and (3-29) reduce to:

$$\omega^2 - \frac{k^3\sigma}{\rho}\tanh\left(\frac{k\tau}{2}\right) = 0 \qquad \text{Symmetric Case} \qquad (3\text{-}30)$$

$$\omega^2 - \frac{k^3\sigma}{\rho}\coth\left(\frac{k\tau}{2}\right) = 0 \qquad \text{Asymmetric Case} \qquad (3\text{-}31)$$

These two equations clearly have two real roots each. Therefore, this analysis predicts complete stability for any disturbance in the flat area of the sheet. This is in agreement with the work done by Taylor. It is possible in this case to solve these equations for ω and consequently predict the phase velocity for each case.

Solving equations (3-30) and (3-31) for ω yields:

$$\omega = \sqrt{\frac{k^3\sigma}{\rho}\tanh\left(\frac{k\tau}{2}\right)} \qquad \text{Symmetric Case} \qquad (3\text{-}32)$$

$$\omega = \sqrt{\frac{k^3\sigma}{\rho}\coth\left(\frac{k\tau}{2}\right)} \qquad \text{Asymmetric Case} \qquad (3\text{-}33)$$

Thus, the wave velocities can be calculated as:

$$c_{sy} = \frac{\omega}{k} = \sqrt{\frac{k\sigma}{\rho}\tanh\left(\frac{k\tau}{2}\right)}$$

$$c_{asy} = \frac{\omega}{k} = \sqrt{\frac{k\sigma}{\rho}\coth\left(\frac{k\tau}{2}\right)}$$

where c_{sy} and c_{asy} are the symmetric and asymmetric wave velocities, respectively. Taking the limit as τ goes to zero results in:

$$c_{sy} = \sqrt{\frac{k\sigma}{\rho}\frac{k\tau}{2}} = k\sqrt{\frac{\sigma\tau}{2\rho}} = \frac{2\pi}{\lambda}\frac{\tau}{2}\sqrt{\frac{2\sigma}{\rho\tau}} = \frac{\pi\tau}{\lambda}u_e \tag{3-34}$$

$$c_{asy} = \sqrt{\frac{k\sigma}{\rho}\frac{2}{k\tau}} = \sqrt{\frac{2\sigma}{\rho\tau}} = u_e \tag{3-35}$$

The velocity of the symmetrical waves is still a function of the wavelength. The velocity of the asymmetrical waves is independent of the wavelength and equal to the edge velocity. Thus the asymmetrical waves are propagated without any dispersion. In a sheet moving with velocity w_0 the asymmetric waves will appear at rest if lines of constant phase are at an angle ψ' to the direction of flow, provided:

$$\sin\psi' = \frac{u_e}{w_0} \tag{3-36}$$

But if the angle the sheet edge makes with the z-direction is ψ then:

$$\tan\psi = \frac{u_e}{w_0} \tag{3-37}$$

Thus, for a long sheet, high w_0, these two relations can be simplified to:

$$\psi' \approx \frac{u_e}{w_0}$$

and

$$\psi \approx \frac{u_e}{w_0}$$

Therefore, for a long sheet the asymmetric waves are parallel to the sheet edge. The velocity of the symmetric waves is still a function of the wavelength of the disturbance. Therefore the symmetrical waves appear as a set of parabolas on the sheet.

Figures 3-2 and 3-3 show actual photographs of the sheet. In Figure 3-2 waves are clearly visible that are parallel to the edges of the sheet. These are representative of the asymmetric waves. In Figure 3-3, there is clearly a set of parabolic shaped waves emanating from a single point. These are representative of the symmetric waves.

Figure 3-2 Photograph of Asymmetric Waves on the Sheet

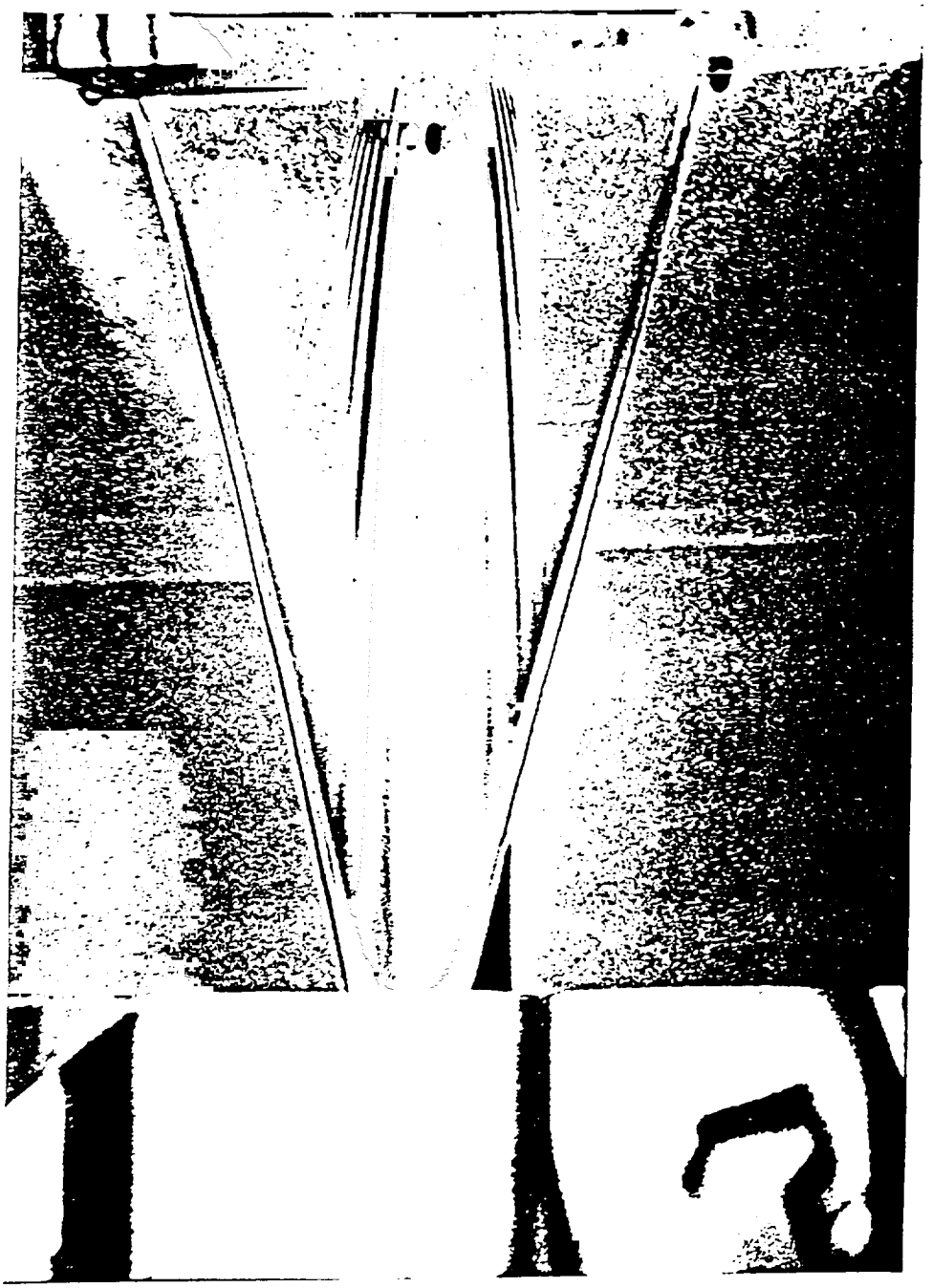

Figure 3-3 Photograph of Symmetric Waves on the Sheet

Now we will consider what happens if the velocities are not zero and the sheet is not flat. If it is assumed that $v_{s,0}$ is steady then from equation (3-3) it may be written that:

$$v_{s,0} = u_{s,0}\frac{\partial s_0}{\partial x} \tag{3-38}$$

Substituting equation (3-38) into equations (3-26) and (3-29) results in:

$$(\omega')^2 + iku_{s,0}\frac{\partial s_0}{\partial x}\tanh(ks_0)\omega' + \frac{k^3\sigma}{\rho'}\left(i\frac{\partial s_0}{\partial x} - \tanh(ks_0)\right) = 0 \qquad \text{Symmetric Case} \quad (3-39)$$

$$(\omega')^2 + iku_{s,0}\frac{\partial s_0}{\partial x}\coth(ks_0)\omega' + \frac{k^3\sigma}{\rho'}\left(i\frac{\partial s_0}{\partial x} - \coth(ks_0)\right) = 0 \qquad \text{Asymmetric Case} \quad (3-40)$$

Rewriting equations (3-39) and (3-40) in terms of the following variables

$$X = ks_0,\ Y = \frac{\omega' s_0}{u_{s,0}},\ \gamma = \frac{\sigma}{\rho' u_{s,0}^2 s_0} \qquad (3-41)$$

results in:

$$Y^2 + i\frac{\partial s_0}{\partial x}X\tanh(X)Y + \gamma X^3\left(i\frac{\partial s_0}{\partial x} - \tanh(X)\right) = 0 \qquad \text{Symmetric Case} \quad (3-42)$$

$$Y^2 + i\frac{\partial s_0}{\partial x}X\coth(X)Y + \gamma X^3\left(i\frac{\partial s_0}{\partial x} - \coth(X)\right) = 0 \qquad \text{Asymmetric Case} \quad (3-43)$$

Taking the limit of equation (3-42) as X, the thickness, goes to zero results in:

$$Y^2 + i\frac{\partial s_0}{\partial x}X^2Y + \gamma X^3\left(i\frac{\partial s_0}{\partial x} - X\right) = 0$$

or,

$$Y^2 = 0 \qquad \text{Symmetric Case} \quad (3-44)$$

Taking the limit of equation (3-43) as X goes to zero results in:

$$Y^2 + i\frac{\partial s_0}{\partial x}\frac{X}{X}Y + \gamma X^3\left(i\frac{\partial s_0}{\partial x} - \frac{1}{X}\right) = 0$$

or,

$$Y = -i\frac{\partial s_0}{\partial x} \qquad \text{Asymmetric Case} \quad (3-45)$$

Therefore, the sheet is completely stable in the symmetric mode but not in the asymmetric mode. In the asymmetric mode, in the limiting case, ω can be found by substituting equation (3-45) and (3-41) into equation (3-24) as:

$$\omega = -\frac{iu_{s,0}}{s_0}\frac{\partial s_0}{\partial x} + ku_{s,0}$$

or, making use of equation (3-38):

$$\omega = -\frac{iv_{s,0}}{s_0} + ku_{s,0}$$

Therefore the imaginary part of ω is equal to:

$$\omega_i = -\frac{v_{s,0}}{s_0} \qquad \text{Asymmetric Case} \quad (3\text{-}46)$$

Since s_0 is always positive, it stands that anywhere $v_{s,0}$ is negative ω_i is positive and the solution for s is unstable to an asymmetric disturbance. Due to the swirling effects shown in Figure 3-2, it can be seen that the cylinder might be unstable near where it connects to the sheet. In this area, s is approaching zero and v_s is negative.

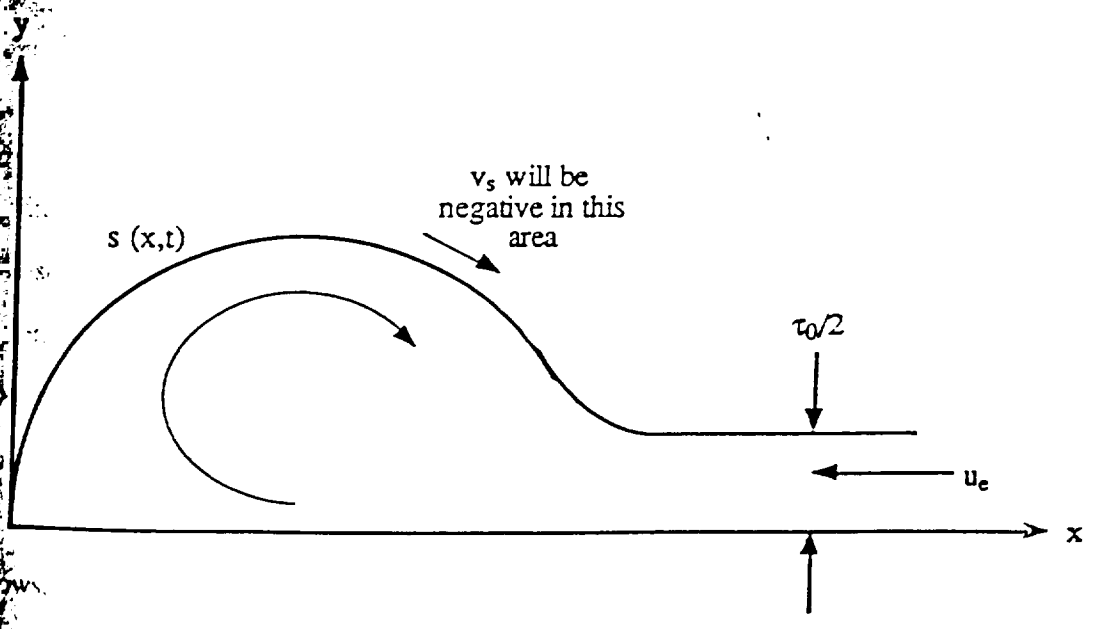

Figure 3-4 Possible Cross-Sectional Shape and Flow Field

Chapter 4

Description of Experimental Apparatus and Study of Hole Formation

A test rig for producing a liquid sheet of silicon oil in a vacuum at NASA Lewis Research Center was constructed previous to this study. This facility was constructed to study the fluid dynamics and emissivity of a thin liquid sheet. This test rig produces a relatively large liquid sheet, on the order of ten feet long. The sheet was contained in a solid steel tank in order to hold a vacuum. The only way of viewing the sheet was to either look through small windows at the top of the tank or look at the videos produced by a small camera with the ability to move up and down and around inside the tank, either way only a small portion of the sheet was visible at any one time.

The sheets formed in this rig appeared to be unstable. That is, when the sheet was observed it would appear to flicker. The sheet also would splatter near the bottom, making it virtually impossible to place a probe near the bottom of the sheet to take any temperature measurements to determine the emissivity. An investigation was undertaken in order to determine the source of this instability. High speed film loops were taken of the sheet. Observation of these high speed film loops revealed that holes formed in the sheet and that they grew as they went down the sheet.

In order to further investigate the formation of these holes and to study liquid sheet flows, three small scale test rigs were made. The sheets in these test rigs were formed with water, in air, and under the influence of gravity. The main advantage the these test rigs was that the entire sheet was visible at all times.

4.1 - Operation of the Small Scale Test Rigs

A schematic of the general design of the small scale test rigs is shown in Figure 4-1. The test rigs basically consist of a plenum or tank with a small slit in the bottom. When the tank is pressurized with water, the water is forced through the slit and the sheet forms.

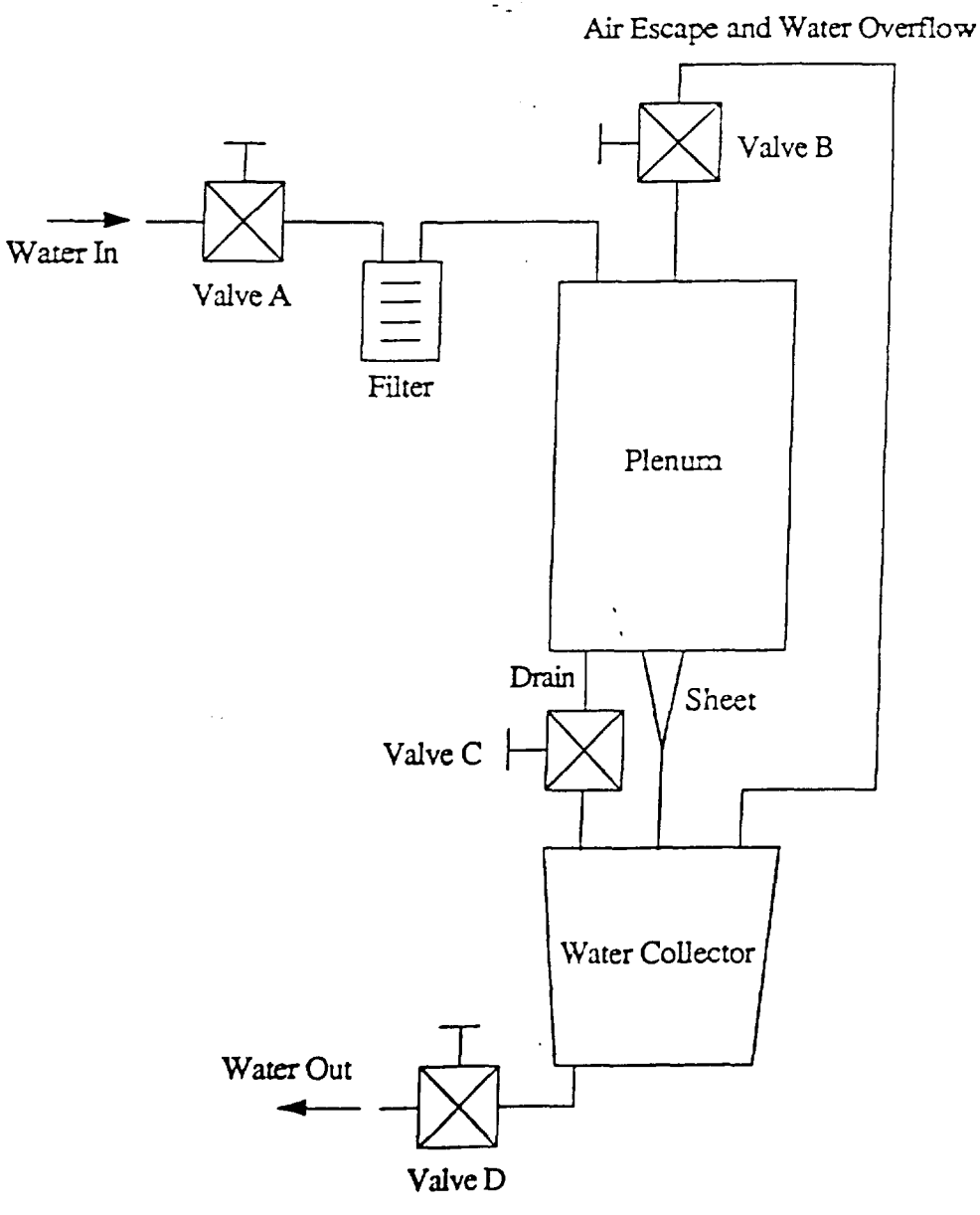

Figure 4-1 Schematic of the Small Scale Test Rig

The water from the sheet is then collected in a bucket or water collector which is equipped with a drain.

Tap water flows into the system through Valve A. Valve A is used to control the mass flow rate through the system and the pressure in the plenum. After the water flows through Valve A, the water is ran through a filter rated to remove any particulates larger than 10 μm. During the time the plenum is filling up with water, Valve C is shut and Valves B and D are open. Valve B allows for air to escape from the plenum during the fill-up time. Once the tank is full, water flows out through Valve B. At this time, Valve B is closed and the plenum begins to pressurize and a liquid sheet begins to form. The water from the overflow and the liquid sheet is collected in the water collector. Valve D is almost always left open, when it is closed water collects in the bucket and mass flow rate measurements can be obtained. When the testing is over, Valve A is closed and Valves B and C are opened to allow for water to drain out of the tank and air to enter the tank.

4.2 - Differences in the Three Small Scale Test Rigs

The differences in the three test rigs are due to the size of the plenums and the size of the slits that they run with. In the first test rig, the volume of the plenum was 66 in^3. The slits all had widths of 1.345 in. and thicknesses of either 0.0021 in., 0.0032 in., or 0.0040 in. The second test rig used the same three slits as the first, but the volume of its plenum was 1,900 in^3. The third test rig had the unique feature of an adjustable thickness on the slit. The slits on this test rig were 8 in. long and the thicknesses were adjustable from 0.0200 in. to 0.0015 in. Also, an impediment could be placed in the slit in order to form sheets less than 8 in. wide. The volume on this plenum was 3,910 in^3.

Figure 4-2 is a photograph of the third small scale test rig, showing the large plenum and the sheet at the base of the plenum. Figure 4-3 shows a close-up photograph of the adjustable slit from the third test rig. The slit is 8 in. long and the positioner has a

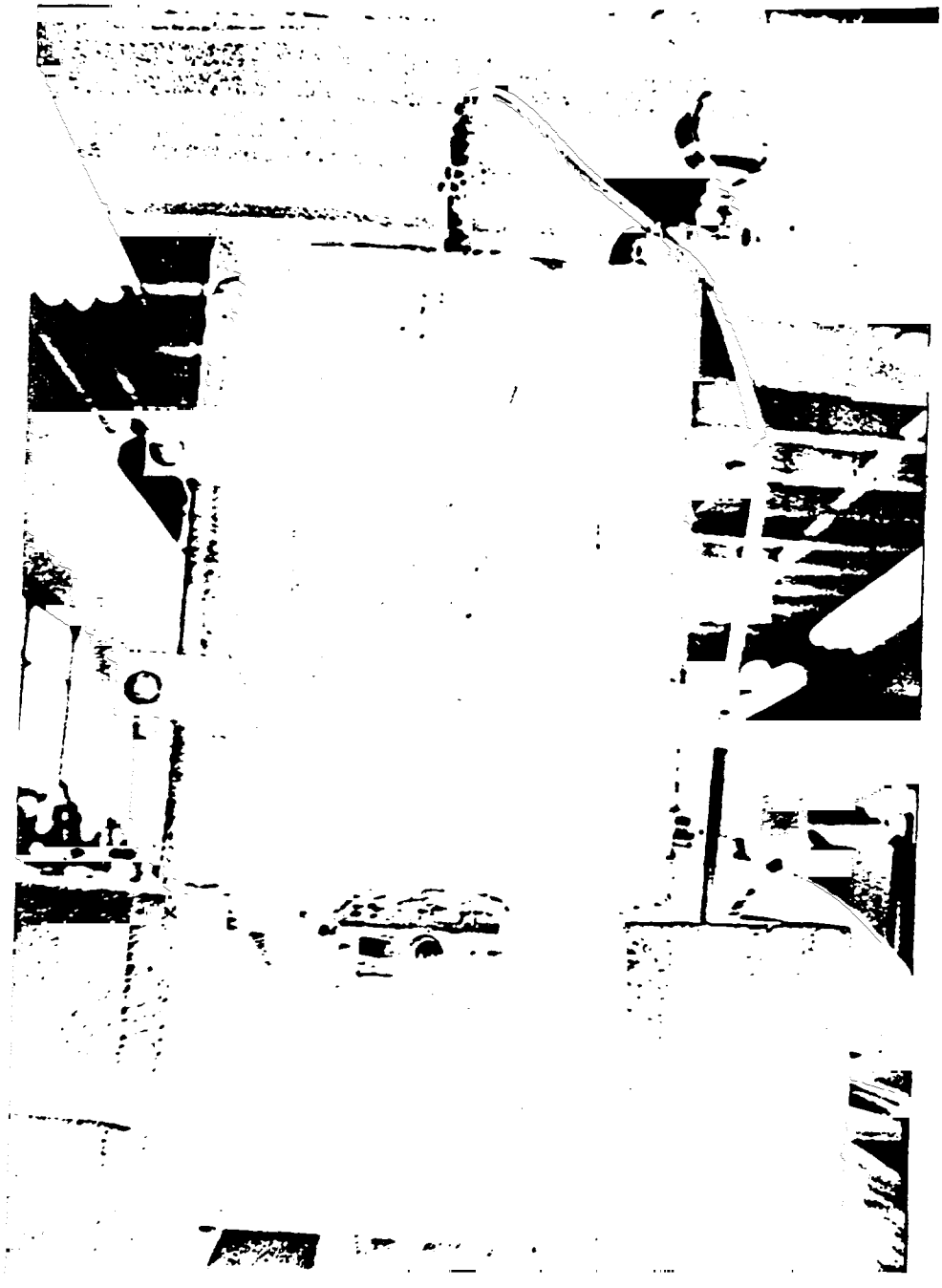

Figure 4-2 Photograph of the Third Small Scale Test Rig

digital readout, capable of showing the thickness of the slit to accuracy of 0.00005 in. Since it was necessary to produce both sides of the slit 8 in. long, parallel, and to the highest possible degree of precision there was a great amount of time spent in the machining of this slit.

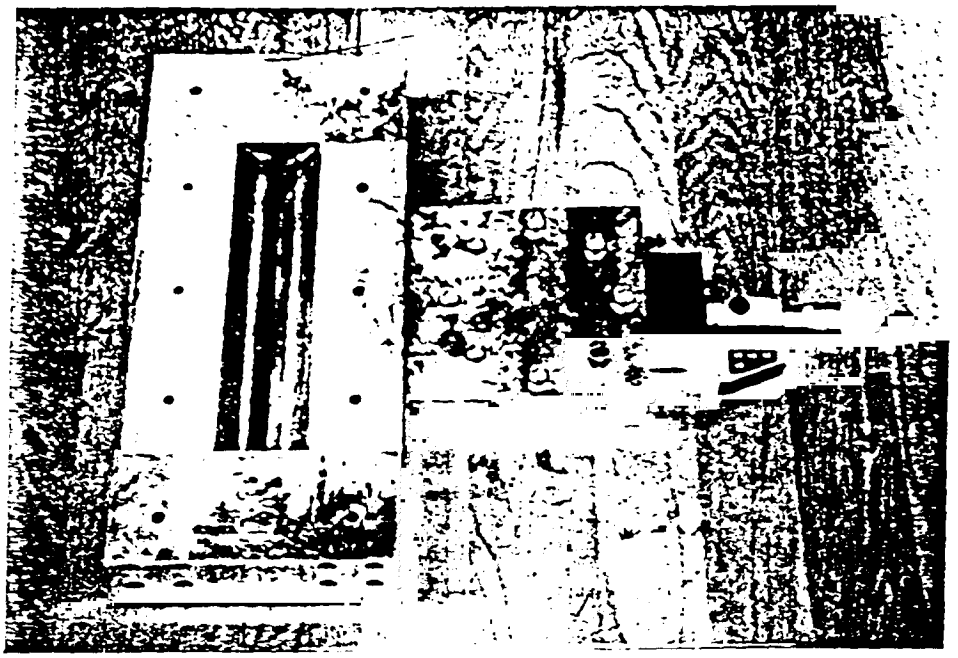

Figure 4-3 Photograph of the Adjustable Slit

4.3 - Experimental Procedure for Determining the Surface Area Lost Due to Hole Formation

The first test rig, equipped with the 0.0032 in. thick slit, was used for determining the surface area lost due to hole formation. The photographic technique employed for determining the surface area lost due to hole formation is shown in Figure 4-4. A camera was set up directly in front of the sheet and a strobe light was set up off center behind the sheet, the dashed line represents the line of sight of the camera. The strobe was placed off center so the area directly behind the sheet would not be flooded with light. The camera used was a Pentax KX and the film was Kodak TMAX400. The shutter speed on the camera was set to 1/60 of a second and the strobe was set to 18,000 flashes per minute. This resulted in there being 5 images of the sheet on each frame of film. Therefore, it was possible to see an image of a hole near the top of the sheet and see four consecutive images of the same hole further down the sheet all on one photograph. Figure 4-5 shows a typical

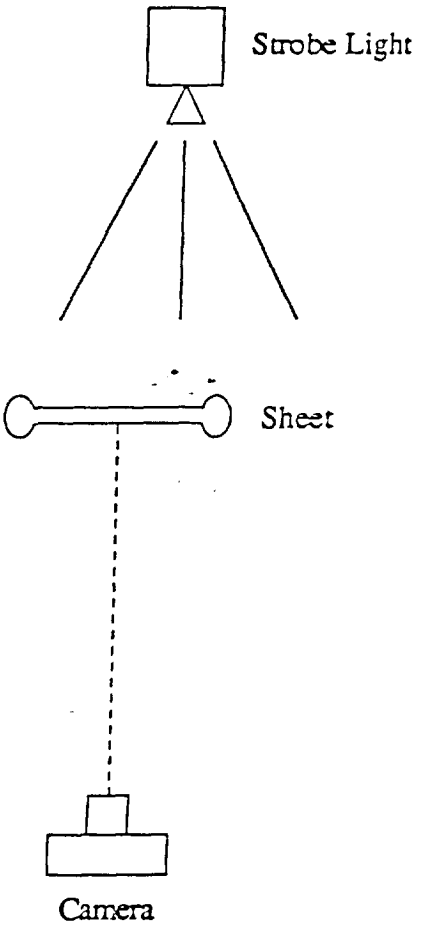

Figure 4-4 Top View of the Experimental Setup for Hole Formation

one of these photographs, showing an image of a hole near the top of the sheet and three more consecutive images of the same hole as it goes through the sheet.

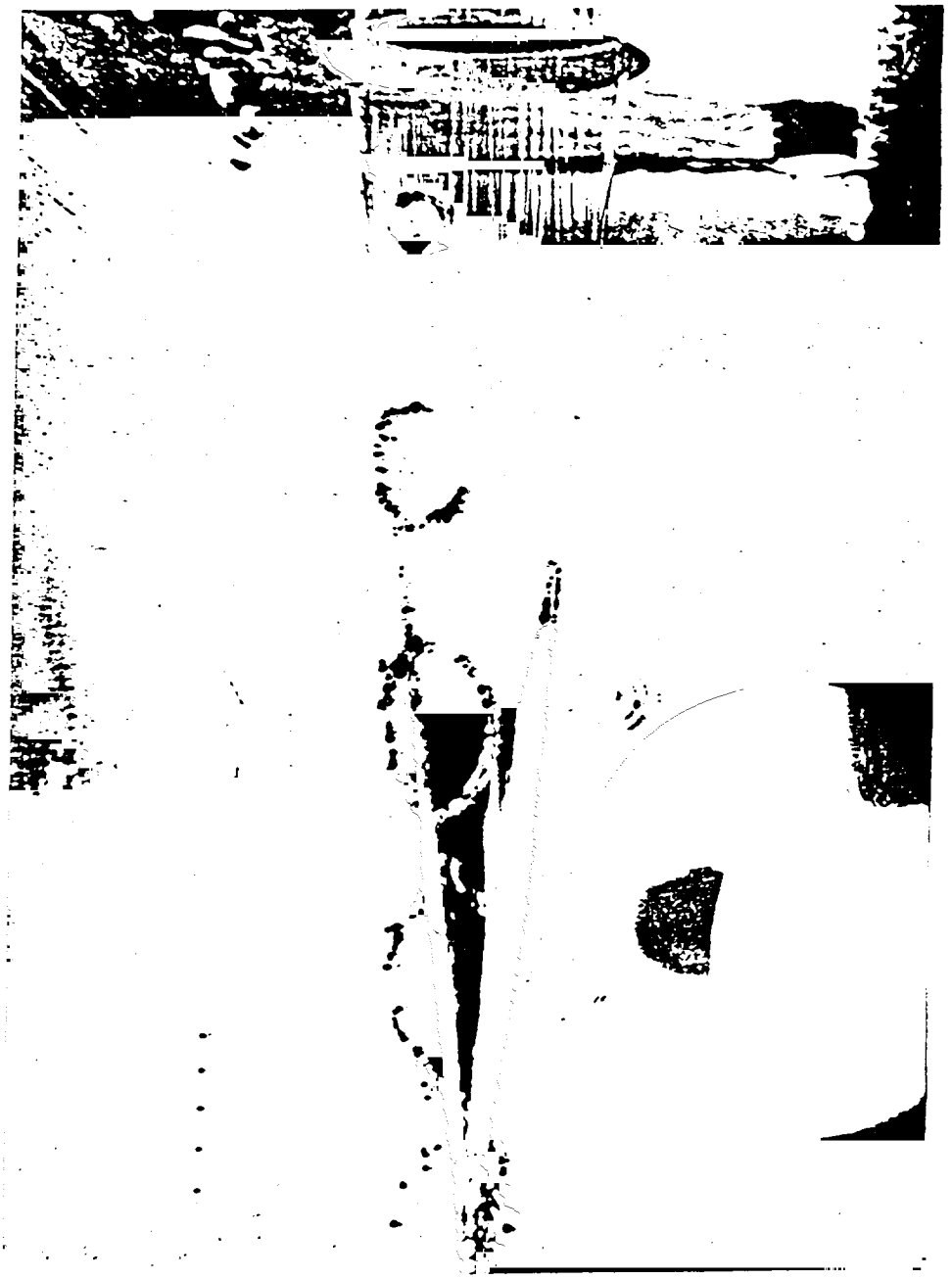

Figure 4-5 Photograph of a Sheet Experiencing Hole Formation

Slides were made of each of these photographs. These slides were then projected on to a digitizing pad. The outlines of the sheet and the holes were then digitized and the areas of the sheet and the holes were computed using the Autocad® software package. From these areas the percent of surface area lost could be calculated. This was done for a number of sheet lengths and operating pressures. The results are shown in Figure 4-6.

Figure 4-6 clearly shows the random appearance of holes in the sheet. Even though there was a general increase in surface area lost as the pressure was increased, there also

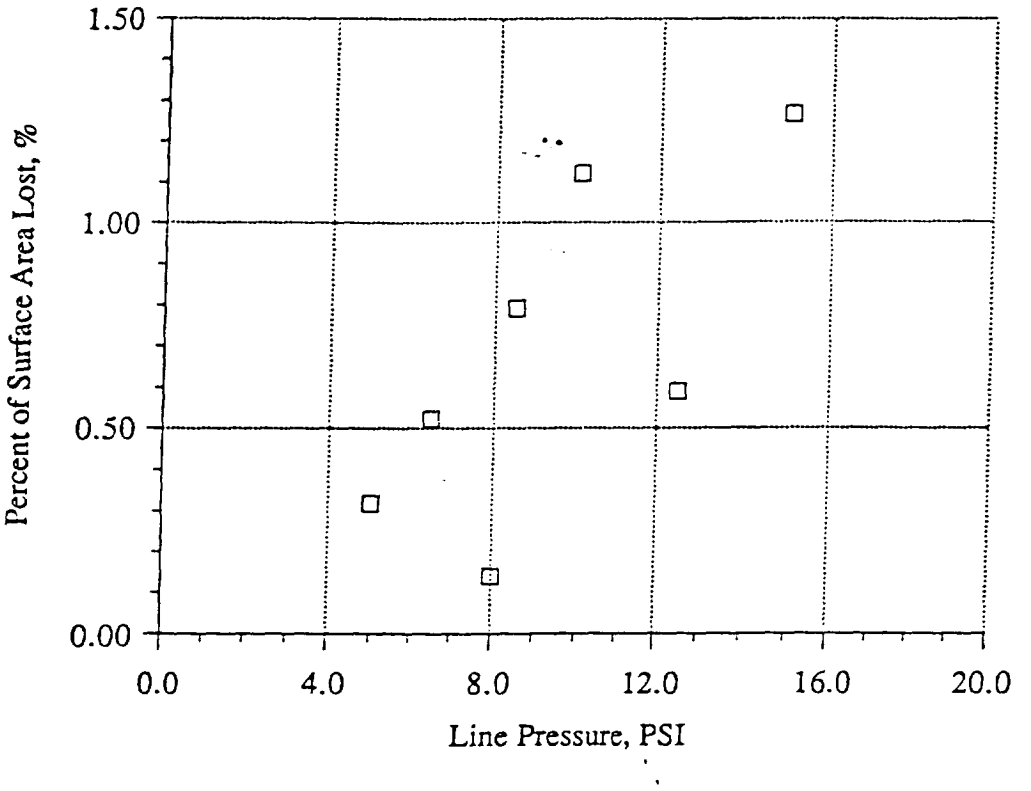

Figure 4-6 Surface Area Lost vs. Line Pressure for the First Test Rig, $\tau = 0.0032$ in.

were distinct exceptions to this rule. This led to the hypothesis that the cause of the holes was not directly linked to the fluid dynamics of the sheet flow alone. In addition, the holes never exhibited any pattern for where they appeared. Holes appeared on the left, right, and center of the sheet. Due to the apparent random nature of their occurrence, it was suspected that upstream disturbances might be the cause of the holes.

For this reason, the second test rig was constructed. With such a large plenum it was assured that the water above the slit would be nearly stagnant and the pressure fluctuations would be greatly minimized. When photographs were taken of the sheet with the new plenum attached it was revealed that no holes were ever formed for all the

conditions tested.

Thus it was concluded that upstream fluctuations were the cause of the hole formation. This finding necessitated the construction of a new plenum for the test rig at NASA Lewis. Since the test rig at NASA was undergoing renovations the experiments performed on the liquid sheet and the data presented in the following chapters were generated by the second and third small scale test rigs.

Chapter 5
Experimental Investigation of Liquid Sheet Flow

Three interesting experimental studies were conducted on liquid sheet flows. In t first, the sheet length over slit width ratio was determined for a number of slit sizes and e velocities. The results from this could be compared to length over width values calculate in Chapter 2, Section 1. In the second study, the widths and thicknesses of the edge cylinders were measured and compared to the computer generated results of Chapter 2, Section 2. In the third study the effects of air resistance on the sheet was studied.

5.1 - Determining the Sheet Length Over Slit Width Ratio

The second test rig, equipped with the 0.0021 in. and 0.0032 in. slits, was used f calculating the sheet length over slit width ratio. Since the water collector on the test rig was set up with a valve on the drain the only equipment necessary for the calculation of the sheet length over the slit width ratio was a millimeter scale. The water collector was graduated with two lines. The volume of water between the two lines was equal to five liters. When, a steady sheet was produced, Valve D (see Figure 4-1) on the water collector was closed. Once the water reached the first line on the inside of the water collector a stopwatch was started. While the bucket was filling up, the length of the sheet was measured with the millimeter scale. When the height of the water reached the second line, the stopwatch was turned off. Knowing the amount of water collected and the time it took to collect it, the volumetric flow rate could be calculated. Thus, the sheet length over slit width ratio could be determined for various flow rates.

5.2 - Determining the Edge Cylinder Cross-Sectional Shape

5.2.1 - Description of Experimental Setup

The photographic technique employed is shown in Figure 5-1. The dashed line represents the line of sight of the camera. A beam splitter and two front faced mirrors were used in order to view both the front and side views of the sheet on the same photograph. The tip of a wire was placed near the sheet edge in order to insure that both images on the photograph were at the same point on the cylinder. Due to the sheet going away from the camera in the side view, there was only one place in this view that was in focus. As a result, the camera was set on the tripod with the ability to move forward and back. Realizing that if the focus on the camera is not adjusted, then any place that is in focus will have the same degree of magnification as any other place that is in focus. It was then possible to take a picture of the front view in focus, tape the lens to insure a constant focal length, and move the camera forwards and back in order to get a number of points along the edge view of the sheet in focus.

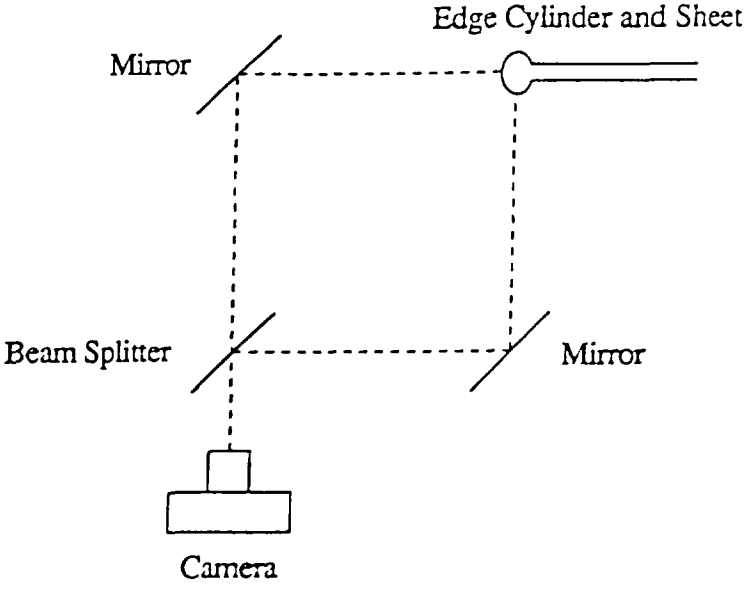

Figure 5-1 Top View of the Photographic Technique for the Edge Cylinders

The camera used was a Nikon F4 equipped with a fully extended bellows and a 200mm Nikon lens, with a +2 diapter close-up lens. Kodak TMAX 400 black and white film was used. The second test rig, equipped with the 0.0021 in., 0.0032 in., and 0.0040 in. slits, was used. One set of data was collected for each slit.

5.2.2 - Experimental Procedure

Once a full, steady liquid sheet was formed, the length of the sheet was measured. The wire tip was placed near the edge cylinder, close to the top of the sheet and the distance from the tip of the wire to the top of the sheet was measured. The camera and mirrors were placed so the wire would have the same length in each view near the bottom of the frame. Two pictures were taken showing both views, and the lens was fixed in place to insure an equal degree of magnification for each picture. Two pictures were then taken showing just the front view for greater clarity. Four or five pictures were taken showing different points in the edge view in focus. This procedure yielded four or five data points along approximately one inch of the edge cylinder.

At this point, a picture of a millimeter scale was taken in order to determine the degree of magnification of the pictures after developing. Then the wire was moved down allowing the top of the next set of photographs to be at the same point as the bottom of the previous set. The height of the wire tip was measured again and the next set of pictures taken. A picture of the millimeter scale was taken after each set of pictures to insure the degree of magnification was not changing. The length of the sheet was periodically measured to insure that the length of the sheet was staying constant.

Enlarged photographs were made for taking the $\bar{r}$ and η_{max} measurements. The pictures of the scale were measured with a millimeter scale to determine the degree of magnification. Knowing the position of the wire tip, the blown-up photograph of the scale could be used to determine the height of the point that appeared to be in focus in each of the

edge shots. The cylinder widths and thicknesses were measured to a resolution of a 64th of an inch.

5.3 - Determining the Effects of Air Resistance on the Sheet

The third test rig, with the adjustable slit, was used for these experiments. It was apparent that for some of the sheets formed by this test rig air resistance would have a very significant affect. In cases where the sheet velocity was high and the sheet thickness was thin, the sheet would catastrophically destruct and form droplets, see Figure 5-2. An attempt was made to determine under what conditions this would happen and to what extent it would happen. The critical length, L_{CR}, is defined as the length from the top of the sheet to the point where the sheet destructs.

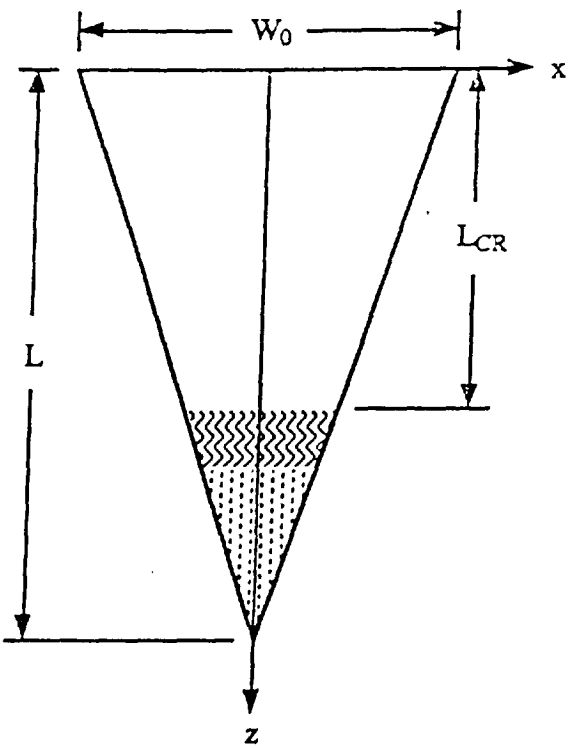

Figure 5-2 Schematic of a Sheet Experiencing Air Resistance Break-up

Once a sheet was formed it was noted if it appeared to destruct due to air resistance or not. If a sheet was fully in tact, its length, L, and thickness, τ_0, were recorded. If the sheet was not fully in tact, its critical length, L_{CR}, would be recorded in addition to its length and thickness. This was done for both 8 and 6 inch wide sheets and a great number of thicknesses and lengths.

Chapter 6
Experimental Results

6.1 - Sheet length Over Slit Width Ratio Results

Knowing the volumetric flow rate and the dimensions of the slit, the exit velocity of the sheet, w_0 (assumed to be uniform), could be calculated by dividing the flow rate by the area of the slit. Assuming the density of water to be 1,000kg/m^3 and the coefficient of surface tension to be 0.0728 N/m, [8], the Weber number could be calculated through the use of equation (2-15). Knowing the dimensions of the slit and the length of the sheet, the sheet length over slit width ratio could be calculated. The results for the sheet length over slit width ratio are plotted against the Weber number in Figure 6-1. The solid line represents the analytical prediction given by equation (2-19). The circular data points are from the 0.0021 in. slit and the square data points are from the 0.0032 in. slit.

6.2 - Edge Cross-Sectional Shape Results

Knowing the dimensions of the slit, the total length of the sheet, and the height at which the data points were taken, the dimensionless cross-sectional area of the edge cylinder, $\overline{A}_c$, could be calculated using equation (2-68). Knowing the degree of magnification and the dimensions of the slit, η_{max} and $\bar{r}$ could be calculated using equation (2-46). These data and the theoretical predictions are shown graphically in Figures 6-2 through 6-4.

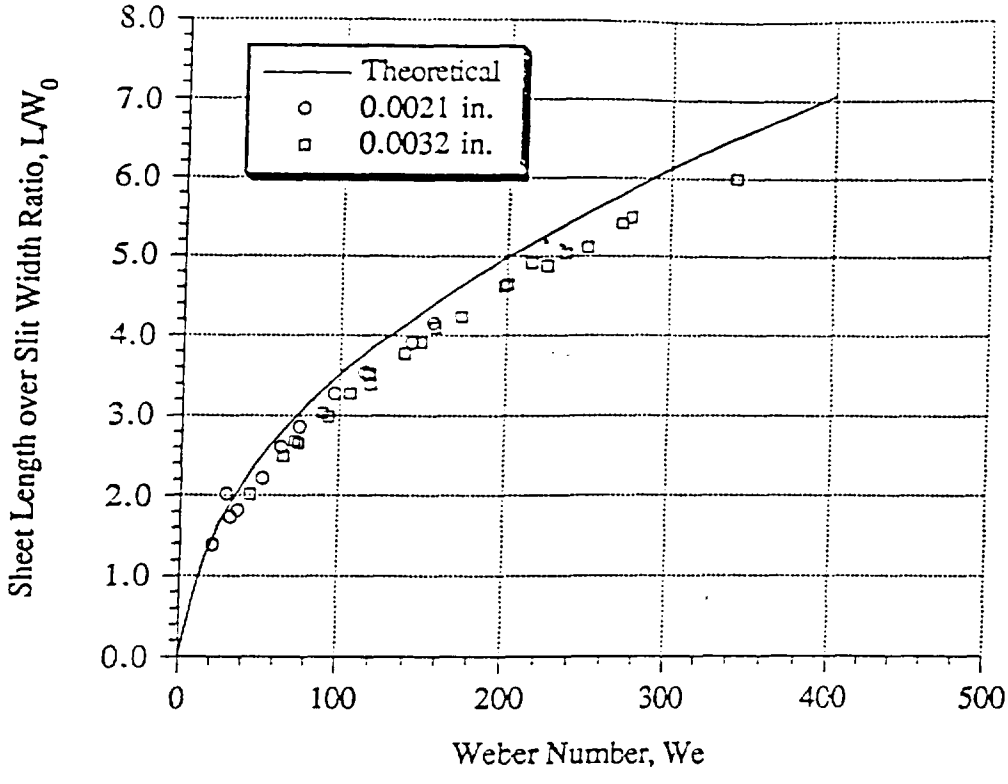

Figure 6-1 Sheet length over Slit Width Ratio vs. Weber Number

Figures 6-2, 6-3, and 6-4 reveal a very interesting phenomenon. The cylinder appears to be oscillating. The cylinder will quickly flatten out and then reform in its basically circular shape. When the cylinder is in its circular shape, the shape is in good agreement with the theoretical predictions. The details of this cycle are shown in Figures 6-5 and 6-6. Figure 6-5 shows a cross-section of the cylinder as one moves down in the z-direction. Figure 6-6 shows the actual photographs of the cylinder.

The cylinder begins in its nearly circular shape, shown in Figure 6-6a. Due to the high curvature where the cylinder connects to the sheet, the cylinder quickly flattens out, shown near the top of Figure 6-6b. This appears in Figure 6-5 as an increase in $\bar{r}$ and a

decrease in η_{max}. Instead of simply regaining its circular shape, the cylinder goes through a rebuilding process where the cylinder has a peanut-like shape. As the area of the cylinder increases η_{max} increases but on the inside of the previous cylinder. This can be seen best a third of the way down the edge view of Figure 6-6b, where the inner part of the cylinder can be seen behind the outer part of the cylinder. It cannot be seen whether the cylinder necks down between the two parts or not. This inner part of the cylinder grows and engulfs the outer part to return to its circular shape. This appears in Figure 6-5 as an increase in η_{max} and a decrease in $\bar{r}$. This is most noticeable in the 0.0040in. slit.

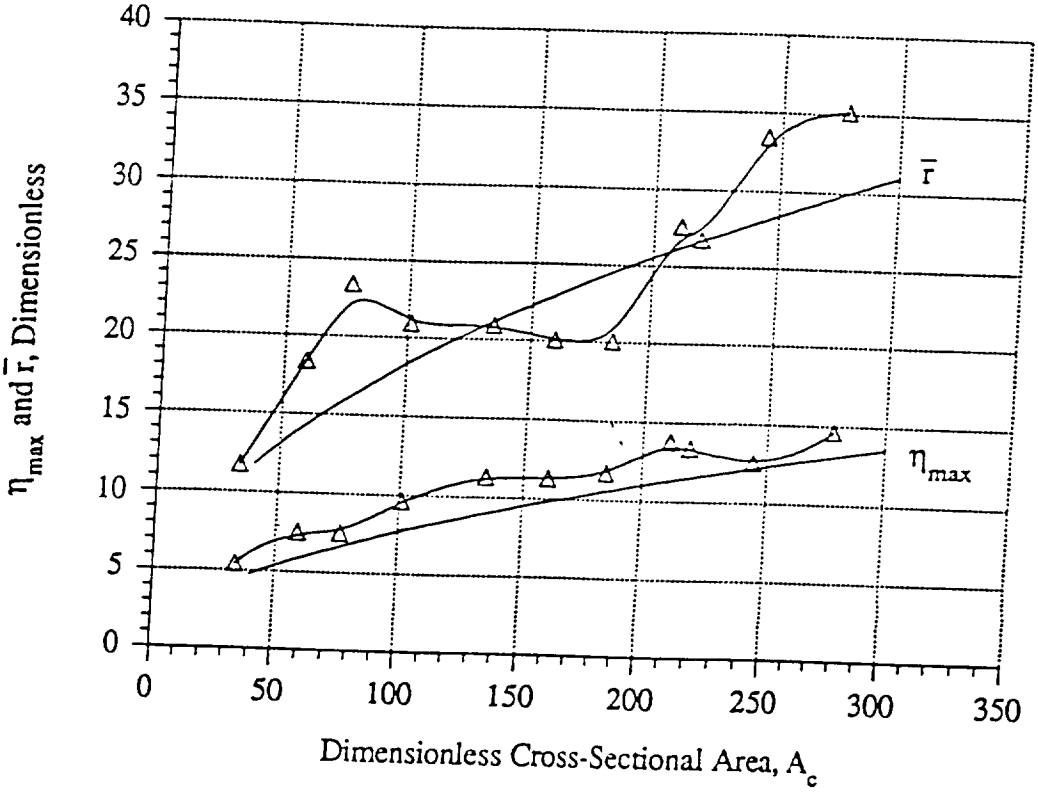

Figure 6-2 η_{max} and $\bar{r}$ vs. Cross-Sectional Area

Theoretical and Experimental for the 0.0021in. Slit

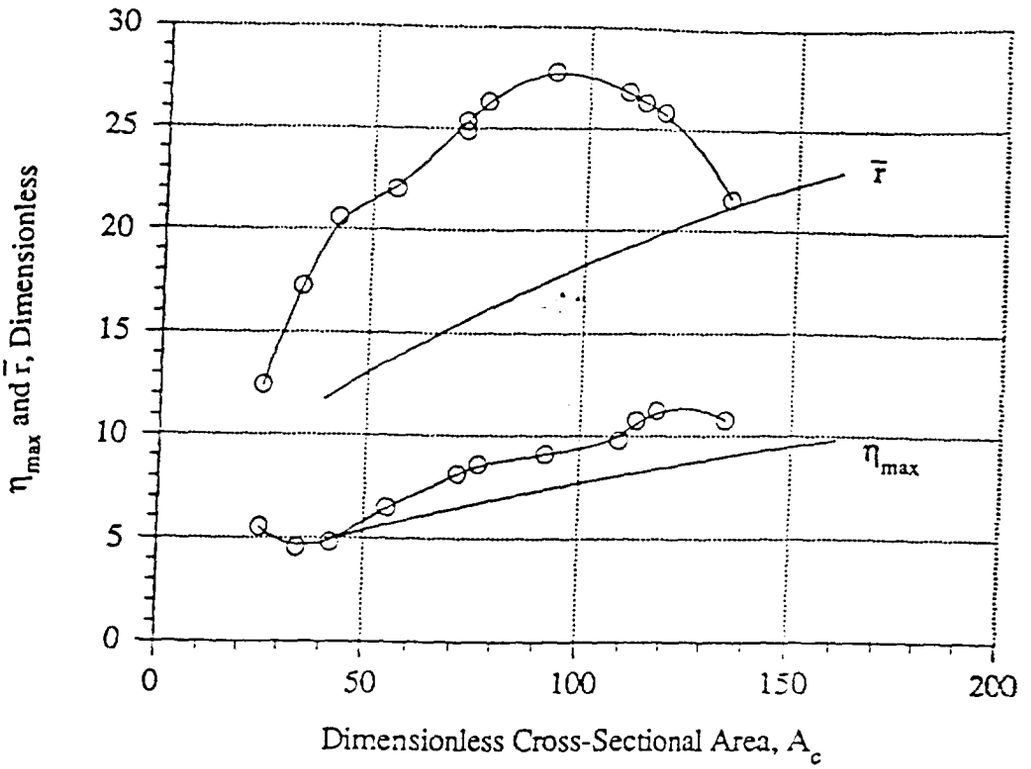

Figure 6-3 η_{max} and $\bar{r}$ vs. Cross-Sectional Area

Theoretical and Experimental for the 0.0032in. Slit

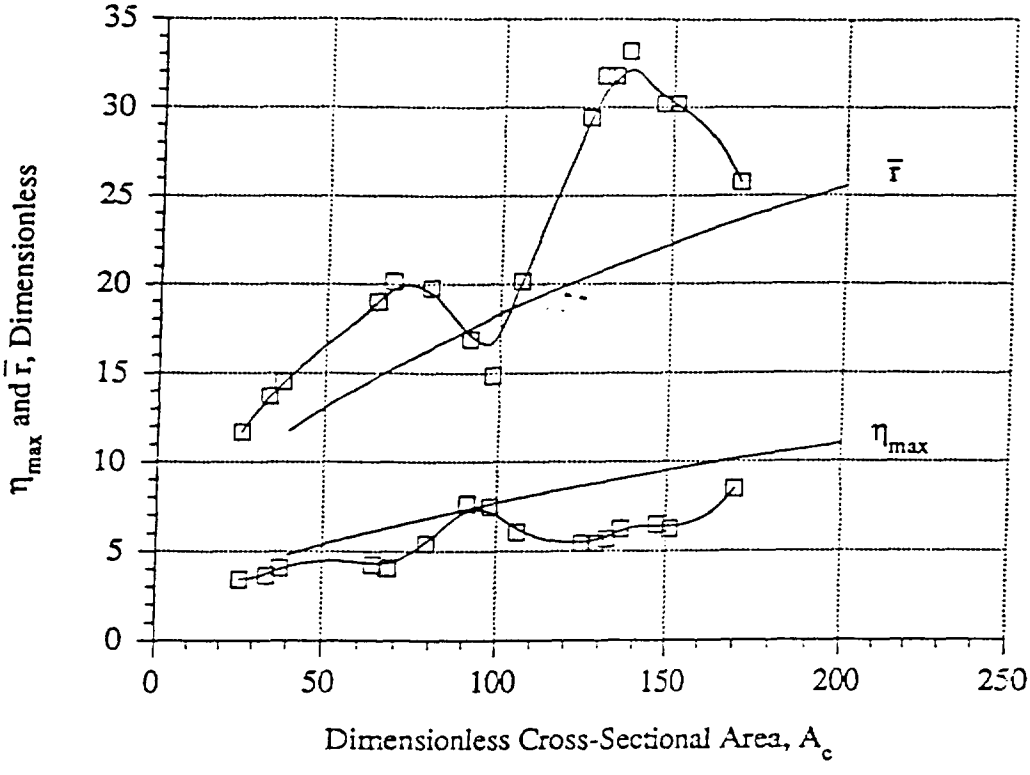

Figure 6-4 η_{max} and $\bar{r}$ vs. Cross-Sectional Area

Theoretical and Experimental for the 0.0040in. Slit

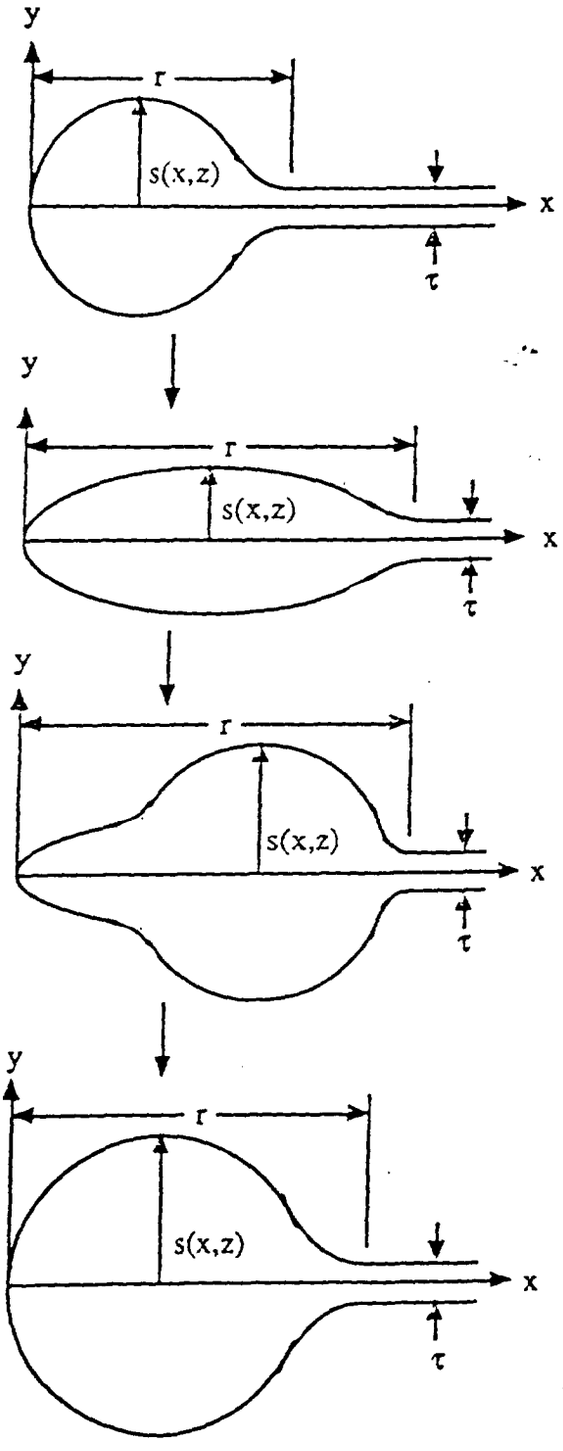

Figure 6-5 Changes in the Cross-Sectional Shape Proceeding in the z-Direction

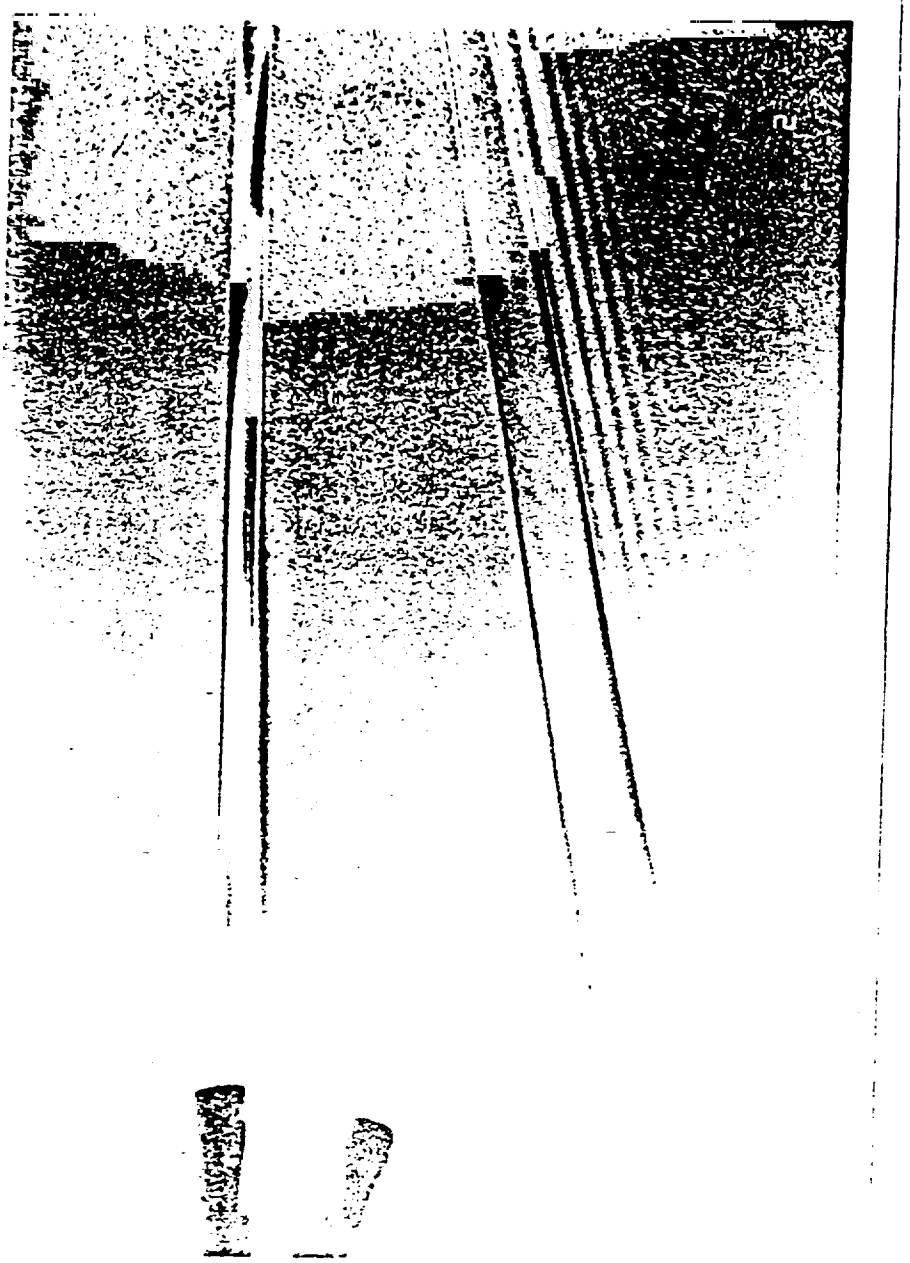

Figure 6-6a Front and Side Views of the Edge Cylinder

Near the Slit Exit, $\tau = 0.0040$ in.

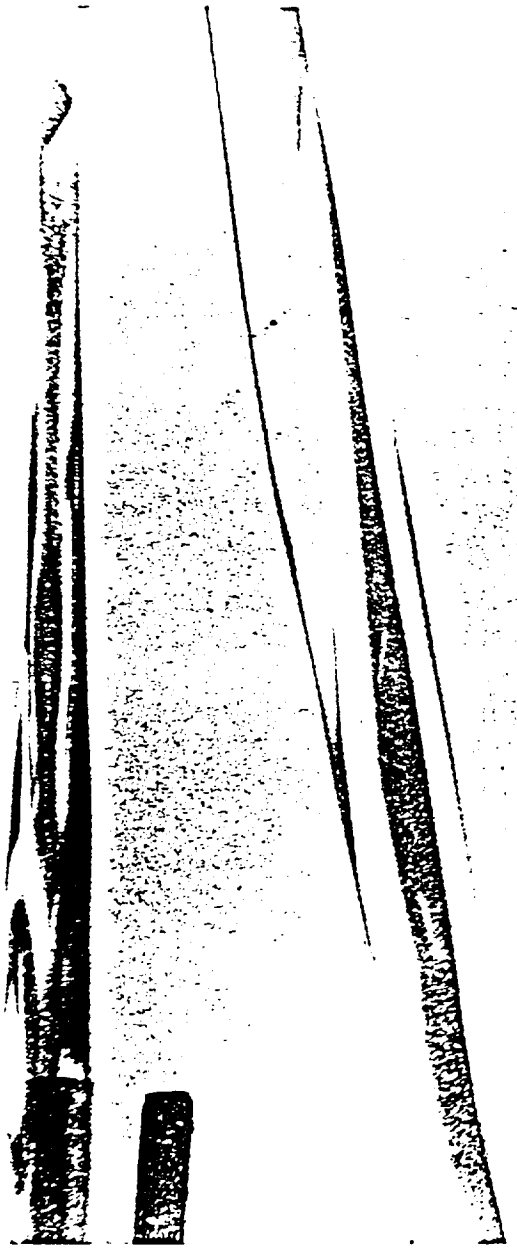

Figure 6-6b Front and Side Views of the Edge Cylinder

Directly Below Figure 6-6a, $\tau = 0.0040$ in.

6.3 - Air Resistance Effects Results

The results for the air resistance effects are shown in Figure 6-7. In Figure 6-7, the sheet length and thickness have each been scaled by the slit width. The critical length has been scaled by the sheet length, in essence giving the percentage of the sheet length that is still in tact. Any combination of W_0/τ_0 and L/W_0 that is below or on the $L_{CR}/L = 1$ line was found to be completely in tact. Any combination above that line was found to be in varied degrees destroyed due to air resistance. It can clearly be seen that in order to run a sheet at a high width to thickness ratio in air one needs to have a shorter sheet.

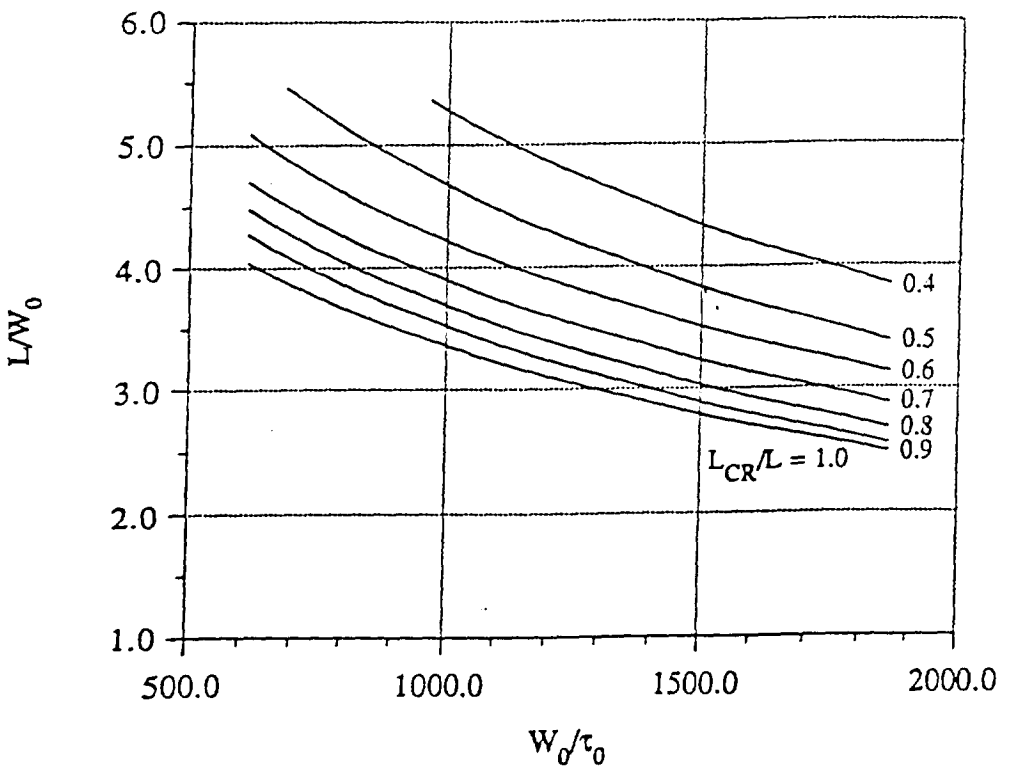

Figure 6-7 Contour Plot for L_{CR}/L

Chapter 7
Conclusion

Theoretical and experimental studies of the fluid dynamics and stability of thin liquid sheet flows have been carried out in this thesis. It was shown that this was a surface tension driven flow. Due to the surface tension, the sheet coalesces to a point after a length L and, due to the conservation of mass, the water collects in the edge cylinders giving the sheet a basically triangular shape. It was shown that gravity had a negligible effect on the shape of the sheet.

A relation was developed linking the sheet length over slit width ratio to the operating parameters of the sheet, namely:

$$\frac{L}{W_0} = \sqrt{\frac{We}{8}}$$

where:

$$We = \frac{\rho w_0^2 \tau_0}{\sigma}$$

Thus the sheet length was found to be proportional to the outlet velocity of the slit. Many experiments were carried out which demonstrated that this relation correctly represents what occurs in thin liquid sheet flow.

A computer program was developed to determine the cross-sectional shape of the edge cylinder given the cross-sectional area of the edge cylinder. Experiments were carried out revealing that the edge cylinder oscillates and that the computer solution was only valid for the limiting case that the edge cylinder was in its basically circular shape.

A stability analysis was performed on a non-planer liquid sheet. This analysis

showed the existence of two different wave formations on the center, flat portion of the sheet. Photographic evidence of the existence of these two wave formations was also found. It was determined that the sheet may be unstable where the y-direction velocity on the surface is negative, see Figure 3-2. It was shown that this is a very likely condition on the edge cylinder near where it connects to the sheet.

A study was conducted to determine the effects of air resistance on the sheet. It was shown that the longer the sheet is, the thicker it needs to be in order to stay in tact.

As to the formation of holes in the sheet, as found at the NASA Lewis test rig, it was found that the holes form due to fluctuations in pressure upstream from the slit. When a large plenum is placed above the slit, hole formation was eliminated.

Appendix A

Derivation of the Total Pressure on a Free Curved Fluid Surface Including Surface Tension

Figure A-1 shows a differential fluid element on the surface of a fluid body. The lengths of the two sides are ds_{yx} and ds_{yz}. The surface is curved, and the radii of curvature are shown as R_{yx} and R_{yz}. The coeficient of surface tension is σ, therefore, the forces connecting this element to the surrounding elements are σds_{yx} and σds_{yz}. Due to the curvature of the element these surface tension forces create a force normal to the surface. Conducting a force balance in the normal direction to the surface results in:

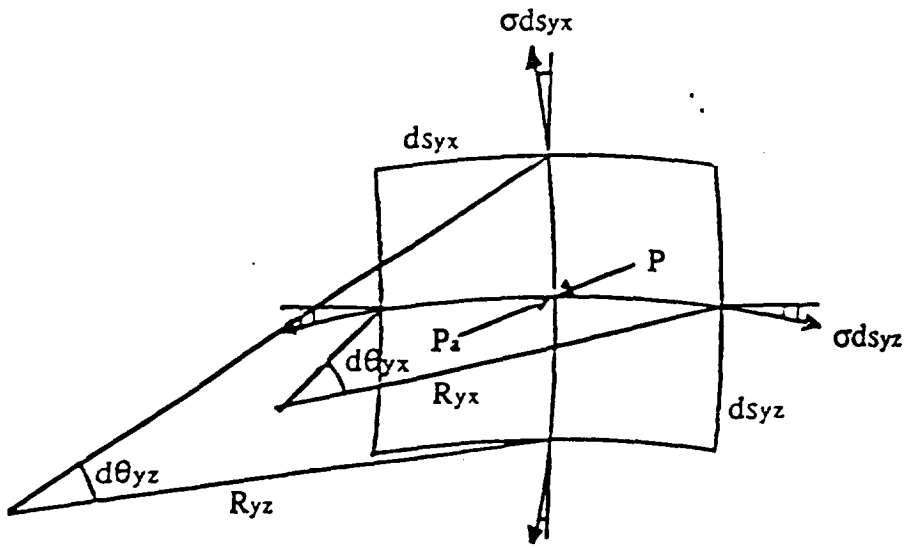

Figure A-1 Differential Surface Element

$$Pds_{yx}ds_{yz} = P_a ds_{yx}ds_{yz} - 2\sigma ds_{yz}\sin\frac{d\theta_{yx}}{2} - 2\sigma ds_{yx}\sin\frac{d\theta_{yz}}{2}$$

Applying the small angle approximation:

$$\sin\frac{d\theta_{yx}}{2} \approx \frac{d\theta_{yx}}{2}$$
$$\sin\frac{d\theta_{yz}}{2} \approx \frac{d\theta_{yz}}{2}$$

results in:

$$Pds_{yx}ds_{yz} = P_a ds_{yx}ds_{yz} - 2\sigma\left(ds_{yz}\frac{d\theta_{yx}}{2} + ds_{yx}\frac{d\theta_{yz}}{2}\right)$$

Dividing by $ds_{yx}ds_{yz}$ results in:

$$P = P_a - \sigma\left(\frac{d\theta_{yx}}{ds_{yx}} + \frac{d\theta_{yz}}{ds_{yz}}\right)$$

or,

$$P = P_a - \sigma\left(\frac{1}{R_{yx}} + \frac{1}{R_{yz}}\right)$$

Since the radii of curvature are defined as [9]:

$$\frac{1}{R_{yx}} + \frac{1}{R_{yz}} = \frac{\frac{\partial^2 s}{\partial x^2} + \frac{\partial^2 s}{\partial z^2}}{\left(1 + \left(\frac{\partial s}{\partial x}\right)^2 + \left(\frac{\partial s}{\partial z}\right)^2\right)^{3/2}}$$

the total pressure is equal to:

$$P = P_a - \sigma\left(\frac{\frac{\partial^2 s}{\partial x^2} + \frac{\partial^2 s}{\partial z^2}}{\left(1 + \left(\frac{\partial s}{\partial x}\right)^2 + \left(\frac{\partial s}{\partial z}\right)^2\right)^{3/2}}\right)$$

Define the surface tension pressure as:

$$P_{ST} = -\sigma\left(\frac{\frac{\partial^2 s}{\partial x^2} + \frac{\partial^2 s}{\partial z^2}}{\left(1 + \left(\frac{\partial s}{\partial x}\right)^2 + \left(\frac{\partial s}{\partial z}\right)^2\right)^{3/2}}\right)$$

Therefore:

$$P = P_a + P_{ST}$$

Appendix B

Program Listings

```
************************************************************************
*   AUTHOR: MATTHEW S. MCMASTER
*   DATE: 12-5-91
*
*   TITLE: FLUDYN
*
*   PURPOSE: DETERMINES SHEET LENGTHS AND THICKNESSES USING THE COMPLETE
*            SOLUTION, INCLUDING GRAVITY, AND COMPARES THEM TO THE NO
*            GRAVITY SOLUTION
*
*   VARIABLE KEY
*
*      WE     :  WEBER NUMBER
*      FR     :  FROUDE NUMBER
*      TAUB   :  TAU-BAR
*      TIMEB  :  TIME-BAR
*      ZB     :  Z-BAR
*      ZBNOG  :  Z-BAR WITH NO GRAVITY
*      NU     :  COEFFICIENT IN THE X-BAR EQUATION
*
*      ALL OTHER VARIABLES, TAUB'S AND DIF'S, ARE JUST DUMMY VARIABLES
*      IN THE ITERATIVE ROUTINE TO SOLVE FOR TAU-BAR
************************************************************************

************************************************************************
*  DECLARE VARIABLES
************************************************************************

      REAL WE,XB,DTAUB,TAUB1,TAUB2,DIF1,DIF2,NU,TAUB,TAUBL,TAUBR,TAUBC,
     +DIFL,DIFR,DIFC,FR,TIMEB,ZB,ZBNOG
      INTEGER I,J

************************************************************************
*  SET STEP SIZE FOR THE ROOT FINDER ROUTINE FOR TAUBAR
************************************************************************

      DTAUB = 0.05

************************************************************************
*  SET HEADINGS FOR OUTPUT
************************************************************************

      WRITE(8,*) '  DATA FOR SHEET LENGTHS AND THICKNESSES FOR WATER'
      WRITE(8,*) '  IN THE SMALL SCALE LSR.'
      WRITE(8,*) ' '
      WRITE(8,*) '  THE FOLLOWING PARAMETERS WERE USED:'
      WRITE(8,*) ' '
      WRITE(8,*) '  SLIT WIDTH:        0.03416 M'
      WRITE(8,*) '  SLIT THICKNESS:    8.128E-5 M'
      WRITE(8,*) '  DENSITY:           1000 KG/M^3'
      WRITE(8,*) '  SURFACE TENSION:   7.282E-2 N/M'
      WRITE(8,*) '  GRAVITY:           9.81 M/S^2'
      WRITE(8,*) ' '
      WRITE(8,*) '  WEBER NUMBERS START AT 20 AND GO THROUGH 500'
      WRITE(8,*) ' '
      WRITE(8,*) '  WEBER      FROUDE    X-BAR      TAUBAR      Z-BAR      Z-
     +BAR'
      WRITE(8,*) '  NUMBER     NUMBER                                      NO
```

```
     +GVAV.'
      WRITE(8,*) ' ------    ------   -----    ------    -----    ---
     +------'
      WRITE(8,*) ' '

*************************************************************************
*  START LOOP FOR WE FROM 20 TO 500 BY 20                               *
*************************************************************************

      DO 10, I = 1,25
      WE = 20.0*I
      FR = 2.6735*W

*************************************************************************
*  DEFINE NU = (FR*SQRT2)/(3*SQRTWE)                                    *
*************************************************************************

      NU = 1.2603*SQRT(WE)

*************************************************************************
*  START LOOP FOR X-BAR FROM 1 TO 0 BY 0.1                              *
*************************************************************************

      DO 20, J = 10,0,-1
      XB = 0.1*J

*************************************************************************
*  FIND Z-BAR WITH NO GRAVITY FOR THE GIVEN WE AND X-BAR                *
*************************************************************************

      ZBNOG = SQRT(WE/8.0) - XB*SQRT(WE/8.0)

*************************************************************************
*  BEGIN THE ITERATIVE ROOT FINDING TECHNIQUE TO FIND TAU-BAR GIVEN WE  *
*  AND X-BAR                                                            *
*************************************************************************

      TAUB1 = 0.05
 30   TAUB2 = TAUB1 + DTAUB
      DIF1 = 1.0 - NU*(TAUB1**(-1.5) + 3.0*TAUB1**(-0.5) - 4.0) - XB
      DIF2 = 1.0 - NU*(TAUB2**(-1.5) + 3.0*TAUB2**(-0.5) - 4.0) - XB
      IF (DIF1 .EQ. 0.0) THEN
          TAUB = TAUB1
      ELSE IF (DIF2 .EQ. 0.0) THEN
          TAUB = TAUB2
      ELSE IF (DIF1*DIF2 .LT. 0.0) THEN
          GOTO 40
      ELSE
          TAUB1 = TAUB2
          GOTO 30
      END IF

 40   TAUBL = TAUB1
      TAUBR = TAUB2
 50   TAUBC = (TAUBL + TAUBR)/2.0
      DIFL = 1.0 - NU*(TAUBL**(-1.5) + 3.0*TAUBL**(-0.5) - 4.0) - XB
      DIFC = 1.0 - NU*(TAUBC**(-1.5) + 3.0*TAUBC**(-0.5) - 4.0) - XB
      DIFR = 1.0 - NU*(TAUBR**(-1.5) + 3.0*TAUBR**(-0.5) - 4.0) - XB
```

```
      IF (ABS(DIFC) .LT. 0.0001) THEN
          TAUB = TAUBC
      ELSE IF (DIFL*DIFC .LT. 0.0) THEN
          TAUBR = TAUBC
          GOTO 50
      ELSE
          TAUBL = TAUBC
          GOTO 50
      END IF

*************************************************************************
*  SUBSTITUTE THE FOUND VALUE FOR TAU-BAR INTO THE TIME-BAR EQUATION    *
*************************************************************************

      TIMEB = (FR*(TAUB**(-1.0) - LOG(TAUB) - 1.0))/4.0

*************************************************************************
*  SUBSTITUTE THE VALUE FOR TIME-BAR INTO THE Z-BAR EQUATION            *
*************************************************************************

      ZB = (TIMEB*TIMEB)/(2.0*FR) + TIMEB
      IF (XB .EQ. 1.0) ZB = 0.0

*************************************************************************
*  OUTPUT THE DATA, END THE LOOPS, AND TERMINATE THE PROGRAM            *
*************************************************************************

 55   FORMAT(1X,F8.2,F10.3,F8.2,F11.5,F11.5,F11.5)
      WRITE(8,55) WE,FR,XB,TAUB,ZB,ZBNOG

 20   CONTINUE
      WRITE(8,*) ' '
 10   CONTINUE

      STOP
      END
```

```
*************************************************************************
*  AUTHOR: MATTHEW S. MCMASTER                                          *
*  DATE: 12-5-91                                                        *
*                                                                       *
*  TITLE: SHAPE                                                         *
*                                                                       *
*  PURPOSE: TO DETERMINE THE CROSS-SECTIONAL SHAPE OF THE SHEET         *
*           ASSUMING PROPORTIONAL SECOND DERIVATIVES                    *
*           USING A FOURTH-ORDER RUNGE KUTTA TECHNIQUE                  *
*                                                                       *
*  VARIABLE KEY                                                         *
*                                                                       *
*  ETA     : ETA ARRAY                                                  *
*  THETA   : DETA/DXI ARRAY                                             *
*  XI      : XI ARRAY                                                   *
*  ACBAR   : AC-BAR                                                     *
*  Q       : TAU/RE                                                     *
*  ALPHA   : ALPHA                                                      *
*  ABAR    : A-BAR                                                      *
*  ETAMAX  : ETA-MAX                                                    *
*  ELLIP   : ELLIPTICITY, 2*ETA-MAX/R-BAR                               *
*************************************************************************

*************************************************************************
*  DECLARE VARIABLES                                                    *
*************************************************************************

      REAL ETA,THETA,XI,ACBAR,Q,ALPHA,ABAR,ETAMAX,DXI,DIF,FETA,FTHETA,
     +F,K1,K2,K3,K4,C1,C2,C3,C4,ELLIP
      INTEGER I,J
      DIMENSION ETA(0:6000),THETA(0:6000),XI(0:6000)

*************************************************************************
*  SET ACBAR, Q, ALPHA, AND THE XI ARRAY                                *
*************************************************************************

      ACBAR = 2000.0
      Q = 1.1952/ACBAR**0.3813
      ALPHA = -0.7571 + 0.1206*LOG(ACBAR)
      DXI = 0.05
      DO 2, I = 0,6000
          XI(I) = I*DXI
  2   CONTINUE

*************************************************************************
*  USING THE RUNGE-KUTTA TECHNIQUE DETERMINE THE ETA AND THETA ARRAYS   *
*************************************************************************

  1   ETA(0) = 0.0
      ETA(1) = (DXI*((4.0*(1+ALPHA))/Q - DXI))**0.5
      THETA(0) = 0.0
      THETA(1) = ((2.0*(1.0+ALPHA))/Q - DXI)/ETA(1)
      ABAR = (ETA(1)*DXI)/2.0

      DO 10, I = 2,6000
          K1 = THETA(I-1)
          C1 = F(ETA(I-1),THETA(I-1),ABAR,ACBAR,ALPHA,Q)
          K2 = THETA(I-1) + (DXI*C1)/2.0
```

```
      C2 = F(ETA(I-1) + (DXI*K1)/2.0,THETA(I-1) + (DXI*C1)/2.0,ABAR,
     +       ACBAR,ALPHA,Q)
      K3 = THETA(I-1) + (DXI*C2)/2.0
      C3 = F(ETA(I-1) + (DXI*K2)/2.0,THETA(I-1) + (DXI*C2)/2.0,ABAR,
     +       ACBAR,ALPHA,Q)
      K4 = THETA(I-1) + (DXI*C3)
      C4 = F(ETA(I-1) + (DXI*K3),THETA(I-1) + (DXI*C3),ABAR,ACBAR,
     +       ALPHA,Q)
      ETA(I) = ETA(I-1) + DXI*(K1 + 2.0*K2 + 2.0*K3 + K4)/6.0
      THETA(I) = THETA(I-1) + DXI*(C1 + 2.0*C2 + 2.0*C3 + C4)/6.0

      IF (ETA(I) .LT. ETA(I-1) .AND. ETA(I-2) .LT. ETA(I-1) .OR. ETA
     +(I) .EQ. ETA(I-1) .AND. ETA(I-2) .LT. ETA(I-1)) ETAMAX = ETA
     +(I-1)
      IF (ETA(I) .GT. ETA(I-1) .AND. ETA(I-2) .GT. ETA(I-1) .OR. ETA
     +(I) .EQ. ETA(I-1) .AND. ETA(I-2) .GT. ETA(I-1)) GOTO 30

      ABAR = ABAR + DXI*(ETA(I) + ETA(I-1))/2.0

 10   CONTINUE

*************************************************************************
*  CHECK THE BOUNDARY CONDITION THAT AT THE MINIMUM ETA SHOULD EQUAL    *
*  ONE AND CHANGE ALPHA UNTIL ETA DOES EQUAL ONE                        *
*************************************************************************

 30   DIF = 1.0 - ETA(I-1)
      IF (ABS(DIF) .LT. 0.0001) GOTO 35
      ALPHA = ALPHA + DIF/20.0
      GOTO 1

*************************************************************************
*  CHECK THE CONDITION THAT AT THE MINIMUM ABAR SHOULD EQUAL ACBAR AND  *
*  CHANGE Q UNTIL ABAR DOES EQUAL ACBAR                                 *
*************************************************************************

 35   DIF = (ACBAR - ABAR)
      IF (ABS(DIF)/ACBAR .LT. 0.0001) GOTO 37
      Q = Q + DIF/30000.0
      GOTO 1

*************************************************************************
*  CALCULATE THE ELLIPTICITY, OUTPUT THE DATA, AND TERMINATE PROGRAM    *
*************************************************************************

 37   ELLIP = (2.0*ETAMAX)/XI(I-1)
 38   FORMAT (1X,F8.2,F12.4,F12.4)
      WRITE (8,*) 'THE FOLLOWING ARE THE RESULTS FOR ETAMAX, RBAR, AND'
      WRITE (8,*) '2*ETAMAX/RBAR, GIVEN THE VALUE FOR ACBAR.  ALSO'
      WRITE (8,*) 'GIVEN IS THE VALUES FOR TAU/RE AND ALPHA NECESSARY'
      WRITE (8,*) 'TO OBTAIN THE RESULT.  ALSO GIVEN IS A TABLE OF'
      WRITE (8,*) 'SAMPLE VALUES OF ETA AND DETA/DXI FOR THE SHOWN'
      WRITE (8,*) 'VALUES OF XI.'
      WRITE (8,*) ' '
 40   FORMAT (1X,A,F8.3)
 41   FORMAT (1X,A,F9.4)
 42   FORMAT (1X,A,F10.5)
      WRITE (8,40) 'ACBAR = ',ACBAR
```

```
      WRITE (8,40) 'ETAMAX =',ETAMAX
      WRITE (8,40) 'RBAR =',XI(I-1)
      WRITE (8,41) '2*ETAMAX/RBAR =',ELLIP
      WRITE (8,42) 'TAU/RE =',Q
      WRITE (8,42) 'ALPHA =',ALPHA
      WRITE (8,*) ' '
      WRITE (8,*) '     XI          ETA       DETA/DXI'
      WRITE (8,*) '     --          ---       --------'
      DO 22, J = 0,I-1,20
          WRITE (8,38) XI(J),ETA(J),THETA(J)
22    CONTINUE

      STOP
      END

*************************************************************************
*  FUNCTION F SUBPROGRAM                                                *
*  F IS BASICLY THE EQUATION BEING SOLVED                               *
*************************************************************************

      FUNCTION F(FETA,FTHETA,ABAR,ACBAR,ALPHA,Q)

      REAL FETA,FTHETA,ABAR,ALPHA,Q,F,ACBAR

          F = ((((ABAR*ABAR*(1.0 + FTHETA*FTHETA))/(FETA*FETA*ACBAR
     +     *ACBAR) - Q)*(1.0 + FTHETA*FTHETA)**1.5)/(2.0*(1.0 + ALPHA)))

      END
```

```
************************************************************************
*  AUTHOR: MATTHEW S. MCMASTER                                         *
*  DATE: 12-6-91                                                       *
*                                                                      *
*  TITLE: SHAPE2                                                       *
*                                                                      *
*  PURPOSE: TO DETERMINE THE CROSS-SECTIONAL SHAPE OF THE SHEET        *
*           ASSUMING A CONSTANT SECOND DERIVATIVE                      *
*           USING A FOURTH ORDER RUNGE-KUTTA TECHNIQUE                 *
*                                                                      *
*  VARIABLE KEY                                                        *
*                                                                      *
*  ETA     : ETA ARRAY                                                 *
*  THETA   : DETA/DXI ARAY                                             *
*  XI      : XI ARRAY                                                  *
*  ACBAR   : AC-BAR                                                    *
*  Q       : TAU/RE                                                    *
*  R       : D^2ETA/DZETA^2                                            *
*  ABAR    : A-BAR                                                     *
*  ETAMAX  : ETA-MAX                                                   *
*  ELLIP   : ELLIPTICITY, 2*ETA-MAX/R-BAR                              *
************************************************************************

************************************************************************
*  DECLARE VARIABLES                                                   *
************************************************************************

      REAL ETA,THETA,ABAR,Q,ACBAR,R,DXI,DIF,ETAMAX,F,XI,FETA,FTHETA,
     +K1,K2,K3,K4,C1,C2,C3,C4,ELLIP
      INTEGER I,J
      DIMENSION ETA(0:6000),THETA(0:6000),XI(0:6000)

************************************************************************
*  SET ACBAR, Q, R, AND THE XI ARRAY                                   *
************************************************************************

      ACBAR = 2000.0
      Q = 403.6506/ACBAR**1.3278
      R = -0.4827 + 0.0791*LOG(ACBAR)
      DXI = 0.05
      DO 2, I = 0,6000
          XI(I) = I*DXI
  2   CONTINUE

************************************************************************
*  USING THE RUNGE-KUTTA TECHNIQUE DETERMINE THE ETA AND THETA ARRAYS  *
************************************************************************

  1   ETA(0) = 0.0
      ETA(1) = (DXI*(4.0/Q - DXI))**0.5
      THETA(0) = 0.0
      THETA(1) = (2.0/Q - DXI)/ETA(1)
      ABAR = (ETA(1)*DXI)/2.0

      DO 10, I = 2,6000
          K1 = THETA(I-1)
          C1 = F(ETA(I-1),THETA(I-1),ABAR,ACBAR,R,Q)
          K2 = THETA(I-1) + (DXI*C1)/2.0
```

```
      C2 = F(ETA(I-1) + (DXI*K1)/2.0,THETA(I-1) - DXI*C1/2.0,
     +       ACBAR,R,Q)
      K3 = THETA(I-1) + (DXI*C2)/2.0
      C3 = F(ETA(I-1) + (DXI*K2)/2.0,THETA(I-1) - DXI*C2/2.0,
     +       ACBAR,R,Q)
      K4 = THETA(I-1) + (DXI*C3)
      C4 = F(ETA(I-1) + (DXI*K3),THETA(I-1) + (DXI*C3),
     +       R,Q)
      ETA(I) = ETA(I-1) + DXI*(K1 + 2.0*K2 + 2.0*K3 + K4)/6.0
      THETA(I) = THETA(I-1) + DXI*(C1 + 2.0*C2 + 2.0*C3 + C4)/6.0

      IF (ETA(I) .LT. ETA(I-1) .AND. ETA(I-2) .LT. ETA(I-1) .OR. ETA
     +  (I) .EQ. ETA(I-1) .AND. ETA(I-2) .LT. ETA(I-1)) ETAMAX = ETA
     +  (I-1)
      IF (ETA(I) .GT. ETA(I-1) .AND. ETA(I-2) .GT. ETA(I-1) .OR. ETA
     +  (I) .EQ. ETA(I-1) .AND. ETA(I-2) .GT. ETA(I-1)) GOTO 3

      ABAR = ABAR + DXI*(ETA(I) + ETA(I-1))/2.0

   10 CONTINUE

*****************************************************************
*  CHECK THE BOUNDARY CONDITION THAT AT THE MINIMUM ETA EQUAL ETA *
*  ONE AND CHANGE R UNTIL ETA DOES EQUAL ONE                      *
*****************************************************************

   30 DIF = 1.0 - ETA(I-1)
      IF (ABS(DIF) .LT. 0.0001) GOTO 35
      R = R - DIF/30.0
      GOTO 1

*****************************************************************
*  CHECK THE CONDITION THAT AT THE MINIMUM ABAR SHOULD EQUAL ACBAR *
*  CHANGE Q UNTIL ABAR DOES EQUAL ACBAR                           *
*****************************************************************

   35 DIF = ACBAR - ABAR
      IF (ABS(DIF)/ACBAR .LT. 0.0001) GOTO 37
      Q = Q - DIF/35000.0
      GOTO 1

*****************************************************************
*  CALCULATE THE ELLIPTICITY, OUTPUT THE DATA, AND TERMINATE    *
*****************************************************************

   37 ELLIP = (2.0*ETAMAX)/XI(I-1)
   38 FORMAT (1X,F8.2,F12.4,F12.4)
      WRITE (8,*) 'THE FOLLOWING ARE THE RESULTS FOR ETAMAX, ETA
      WRITE (8,*) '2*ETAMAX/RBAR, GIVEN THE VALUE FOR ACBAR.  ALS
      WRITE (8,*) 'GIVEN IS THE VALUES FOR TAU/RE AND DELTA/RE
      WRITE (8,*) 'NECESSARY TO OBTAIN THE RESULT.  ALSO GIVEN IS
      WRITE (8,*) 'TABLE OF SAMPLE VALUES OF ETA AND DELTA ETA FOR
      WRITE (8,*) 'SHOWN VALUES OF XI.'
      WRITE (8,*) ' '
   40 FORMAT (1X,A,F8.3)
   41 FORMAT (1X,A,F9.4)
   42 FORMAT (1X,A,F10.5)
      WRITE (8,40) 'ACBAR = ',ACBAR
```

```
      WRITE (8,40) 'ETAMAX =',ETAMAX
      WRITE (8,40) 'RBAR =',XI(I-1)
      WRITE (8,41) '2*ETAMAX/RBAR =',ELLIP
      WRITE (8,42) 'TAU/RE =',Q
      WRITE (8,42) 'D^2ETA/DZETA^2 =',R
      WRITE (8,*) ' '
      WRITE (8,*) '     XI          ETA       DETA/DXI'
      WRITE (8,*) '     --          ---       --------'
      DO 22, J = 0,I-1,20
          WRITE (8,38) XI(J),ETA(J),THETA(J)
22    CONTINUE

      STOP
      END

*************************************************************************
*  FUNCTION F SUBPROGRAM                                                *
*  F IS BASICLY THE EQUATION BEING SOLVED                               *
*************************************************************************

      FUNCTION F(FETA,FTHETA,ABAR,ACBAR,R,Q)

      REAL FETA,FTHETA,ABAR,R,Q,F,ACBAR

          F = (((ABAR*ABAR*(1.0 + FTHETA*FTHETA))/(FETA*FETA*ACBAR*
     +    ACBAR) - Q)*(1.0 + FTHETA*FTHETA)**1.5)/2.0 - R

      END
```

Bibliography

1. Taylor, Sir Geoffrey. "The Dynamics of Thin Sheets of Fluid II. Waves on Fluid Sheets." Proceedings of the Royal Society of London 252 (1959) 296-312
2. Dombrowski, N., and R.P. Fraser. "Photographic Investigation into the Disintegration of Liquid Sheets." Phil. Trans. 247 (1954) 101-121
3. Crapper, G.D. "An Exact Solution for Progressive Capillary Waves of Arbitrary Amplitude." Journal of Fluid Mechanics 2 (1957) 532-540
4. Drazin, P.G., and W.H. Reid. Hydrodynamic Stability. Cambridge: Cambridge University Press, 1981
5. Brown, D.R. "A Study of the Behaviour of a Thin Sheet of Moving Fluid." Journal of Fluid Mechanics 10 (1960) 297-305
6. Lin, S.P. "Stability of a Viscous Liquid Curtain." Journal of Fluid Mechanics 104 (1981) 111-118
7. Chubb, Donald L., and K. Alan White, III. Liquid Sheet Radiator. Technical Memorandum, National Aeronautics and Space Administration, Lewis Research Center
8. Avallone, Eugene A., and Theodore Baumeister III. Mark's Standard Handbook for Mechanical Engineers. New York: McGraw-Hill Book Company, 1987.
9. Ayres, Frank Jr. Theory and Problems of Differential and Integral Calculus. New York: McGraw-Hill Book Company, 1964.